Synergistic enhancement of spinal fusion in preclinical models using low-dose rhBMP-2 and stromal vascular fraction in an injectable hydrogel composite

Hye Yeong Lee [a,1] , Seong Bae An [b,c,1] , Sae Yeon Hwang [a] , Gwang Yong Hwang [a] ,
Hye-Lan Lee [a] , Hyun Jung Park [d] , Joongkyum Shin [a] , Keung Nyun Kim [a] , Sung Won Wee [a] ,
Sol Lip Yoon [a] , Yoon Ha [a,e,*]

[a] Spine & Spinal Cord Institute, Department of Neurosurgery, College of Medicine, Yonsei University, Seoul, 03722, Republic of Korea
[b] Department of Neurosurgery, School of Medicine, CHA University, CHA Bundang Medical Center, Seongnam-si, 13496, Gyeonggi-do, Republic of Korea
[c] Graduate School, College of Medicine, Yonsei University, Seoul, 03722, Republic of Korea
[d] Department of Research Center, CGBio., co. Ltd, Seongnam-si, Gyeonggi-do, Republic of Korea
[e] POSTECH Biotech Center, Pohang University of Science and Technology (POSTECH), Pohang, Gyeongbuk, 37673, Republic of Korea

A R T I C L E   I N F O

A B S T R A C T

Spinal fusion surgery remains a significant challenge due to limitations in current bone graft materials, particularly in terms of bioactivity, integration, and safety. This study presents an innovative approach using an injectable hydroxyapatite/β-tricalcium phosphate (HA/β-TCP) hydrogel combined with stromal vascular fraction (SVF) and low-dose recombinant human BMP-2 (rhBMP-2) to enhance osteodifferentiation and angiogenesis. Through a series of in vitro studies and preclinical models involving rats and minipigs, we demonstrated that the hydrogel system enables the sustained release of rhBMP-2, resulting in significantly improved bone density and integration, alongside reduced inflammatory responses. The combination of rhBMP-2 and SVF in this injectable formulation yielded superior spinal fusion outcomes, with enhanced mechanical properties and increased bone mass in both small and large animal models. These findings suggest that this strategy offers a promising and safer alternative for spinal fusion, with strong potential for clinical application.

1. Introduction

Spinal fusion surgery, a widely employed intervention for diverse spinal disorders, involves the fusion of adjacent vertebrae to enhance spinal stability. This surgical approach is used to treat conditions ranging from traumatic spine fractures and metastatic spine tumors to spinal deformities and degenerative spinal diseases, including spinal stenosis, herniated intervertebral discs, spondylolisthesis, and spinal instability [1–3]. Although the autologous bone graft (ABG) remains the gold standard for spinal fusion, it is associated with several limitations, including donor site morbidity, infection risks, and limited graft availability, which often lead to patient discomfort and prolonged recovery times. These drawbacks have prompted the exploration of alternative bone graft substitutes, such as allografts, ceramic-based grafts, demineralized bone matrix, and growth factor-based grafts [4].

Among the alternatives, bone morphogenetic proteins (BMPs), members of the transforming growth factor-beta (TGF-β) superfamily, particularly BMP-2, have gained significant attention for their potent osteoinductive properties [5,6]. However, BMP-2 has a short half-life, requiring an efficient delivery system to maximize its osteogenic potential. Recombinant human BMP-2 (rhBMP-2), commercially available in formats such as rhBMP-2 infused into an absorbable collagen sponge (INFUSETM), has demonstrated fusion rates comparable to ABG in clinical studies [7–10]. Despite these benefits, high-dose rhBMP-2 use has been linked to complications, such as inflammation, ectopic bone formation, osteolysis, and potential tumor formation [11–13]. These adverse effects are often attributed to the initial burst release and the supraphysiologic doses of rhBMP-2 used in many clinical applications. To mitigate these risks, it is crucial to develop a delivery system that can provide sustained, controlled release of rhBMP-2 at lower doses while

maintaining its osteoinductive activity. This would enhance the therapeutic safety profile and broaden the clinical applicability of rhBMP-2.

To address the need for sustained rhBMP-2 release, calcium phosphate-based ceramics, such as hydroxyapatite (HA, $Ca_{10}(PO_4)_6(OH)_2$) and tricalcium phosphate (TCP, $Ca_3(PO_4)_2$), have been widely explored as potential carriers due to their excellent biocompatibility and osteoconductive properties [14,15]. These materials mimic the chemical composition of bone, promoting bone regeneration and osseointegration. In particular, the combination of HA and β-TCP offers a balanced resorption profile, with HA providing long-term structural stability and β-TCP facilitating a gradual release of calcium and phosphate ions essential for bone formation [15–17]. By adjusting the HA/TCP ratio, a controlled degradation rate can be achieved, optimizing the sustained release of rhBMP-2 and supporting the bone remodeling process. This strategy provides a stable environment for bone regeneration, which is critical for effective spinal fusion.

In addition to ceramic carriers, hydrogels have emerged as promising candidates for delivering bioactive factors such as rhBMP-2 in minimally invasive spinal fusion procedures [18,19]. Hydrogels consist of hydrophilic polymer networks that create a biomimetic environment, facilitating cellular infiltration and molecule diffusion [20]. Poloxamer 407 and hydroxypropyl methylcellulose (HPMC) are two biodegradable polymers widely used in pharmaceutical formulations due to their low toxicity, biocompatibility, and controlled release properties [21–25]. These materials, when used in combination, create a hydrogel matrix that prevents the initial burst release of rhBMP-2 and ensures a sustained release over time. This property is essential for reducing the side effects associated with high-dose rhBMP-2 while maintaining its osteogenic activity.

While the sustained release of rhBMP-2 is crucial for enhancing bone formation, successful spinal fusion also requires adequate vascularization to ensure nutrient supply and tissue integration. Adipose-derived SVF, a heterogeneous collection of cells isolated from adipose tissue, has shown great potential in promoting both osteogenesis and angiogenesis [26,27]. SVF contains adipose-derived stem cells (ADSCs) that can differentiate into osteoblasts, as well as endothelial progenitor cells that support angiogenesis [28–31]. Additionally, SVF's anti-inflammatory and immunomodulatory properties make it an attractive candidate for enhancing bone remodeling and tissue healing in spinal fusion procedures. However, despite these promising properties, the synergistic potential of SVF and rhBMP-2 for promoting both bone formation and neovascularization has not been thoroughly investigated, which provides a key motivation for our study.

In a previous study conducted [32], we investigated the feasibility of using a putty-type carrier composed of HA/B-TCP, poloxamer 407, and HPMC to load 500 μg/level and 1000 μg/level of rhBMP-2 in a minipig OLIF model. The results confirmed the predicted outcomes of fusion in both groups at 8weeks. However, the study had limitations due to the absence of a gold standard autologous iliac crest bone graft (ICBG) comparison group. Additionally, other feasibility studies have been conducted at lower rhBMP-2 doses in the SD rat model, as noted in papers by Dr. Kaito [33] Furthermore, we aimed to explore the synergistic effect of low-dose rhBMP-2 on neovascularization and bone differentiation following SVF treatment of bone defects.

Building upon the known limitations of high-dose rhBMP-2, such as its associated risks of inflammation, ectopic bone formation, and other side effects, our study aims to evaluate a safer and more effective approach by combining low-dose rhBMP-2 with SVF. This combination is expected to enhance both osteogenesis and angiogenesis, which are critical processes for successful spinal fusion. In our previous research, a putty-type carrier system composed of HA/β-TCP, Poloxamer 407, and HPMC demonstrated promising outcomes in a minipig oblique lateral interbody fusion (OLIF) model. However, this study lacked direct comparison with the autologous iliac crest bone graft (ICBG), the clinical gold standard.

To address these gaps, this study investigates the synergistic effects

of low-dose rhBMP-2 and SVF through a comprehensive series of experiments. We evaluated their osteogenic and angiogenic properties through in vitro studies, followed by in vivo assessments in rat PLF and minipig OLIF models, providing robust insights into the safety, efficacy, and clinical relevance of this approach. This research not only validates the potential of low-dose rhBMP-2 combined with SVF for bone regeneration but also explores its feasibility as a next-generation biological scaffold for spinal fusion, offering a potentially safer alternative to traditional high-dose BMP-2 therapies.

2. Materials and methods

2.1. Experimental design

This study employed a multi-phase approach to investigate the synergistic effects of low-dose recombinant human bone morphogenetic protein-2 (rhBMP-2) and SVF on spinal fusion, aiming to optimize the clinical application of these materials. The study utilized an injectable bone graft material (BGM) comprising HA granules, β-TCP microspheres, and a hydrogel mixture designed to facilitate the sustained release of rhBMP-2. The BGM was combined with SVF, isolated from the patient's adipose tissue, to enhance osteodifferentiation and angiogenesis, both in vitro and in vivo.

2.1.1. In vitro studies: osteodifferentiation and angiogenesis

The initial phase of the study assessed the osteodifferentiation and angiogenic potential of the combination of rhBMP-2 and SVF using in vitro assays. Human mesenchymal stem cells (hMSCs) and rat SVF cells were cultured individually or in combination. Osteodifferentiation was evaluated by measuring markers such as alkaline phosphatase (ALP) activity, while angiogenesis was assessed through tube formation assays and CD31 expression.

2.1.2. Rat posterolateral fusion (PLF) model: animal surgery

In the second phase, the in vivo effects of BGM combined with rhBMP-2 and SVF were tested using a rat model of posterolateral fusion (PLF). The rats were divided into four groups: a control group with HA/β-TCP alone, and three experimental groups with HA/β-TCP combined with either rhBMP-2, SVF, or both. Following PLF surgery, where the composite bone graft material was implanted at the lumbar level, the rats were observed for 8 weeks. Afterward, they were sacrificed, and spinal tissues were harvested for biomechanical testing and histological analysis to evaluate bone fusion and the quality of the newly formed bone.

2.1.3. Minipig oblique lateral interbody fusion (OLIF) model: clinical translation

The final phase of the study involved a minipig model of oblique lateral interbody fusion (OLIF) to assess the translational potential of the findings. This model closely mimics human spinal fusion surgery, allowing for the evaluation of the clinical applicability of the combined treatment approach. Minipigs are divided into three groups: Autologous Bone Graft (ABG), Novosis Putty™ with rhBMP-2, and Novosis Putty™ with both rhBMP-2 and SVF.

The effectiveness of spinal fusion is measured through kinematic testing, micro-computed tomography (micro-CT), and histological analyses at 8 and 16 weeks post-surgery.

The outcomes of the minipig model are intended to validate the in vitro and rat model findings and provide insights into the potential for clinical application in human spinal fusion procedures.

2.2. Preparation of composite injectable bone graft material (BGM) composition

The composite bone graft material (BGM) was meticulously prepared to ensure reproducibility and consistency across all experiments. The

BGM utilized in this study is a proprietary formulation known as Novosis Putty™, provided by CGBio Co., Ltd (CG Bio Co., Ltd, Seongnam-si, Gyeonggi-do, Republic of Korea). Novosis Putty is a kit product comprising Hydroxyapatite (HA), B-TCP/hydrogels (TH composite), rhBMP-2, and WFI (Water for Injection). The product is designed to be reconstituted into a putty formulation immediately before use by mixing its components. In this product, rhBMP-2 is dissolved in WFI, while HA and B-TCP/hydrogels act as bone graft materials to deliver rhBMP-2. The final Novosis Putty is designed to contain 0.4 mg of rhBMP-2 per volume (cc) of bone graft material. Novosis Putty is an injectable, putty-type bone graft material specifically designed for easy insertion into interbody cages (Fig. 5, A). Its application and formulation have been previously introduced in earlier studies [34–36]. The characteristics of each component are detailed below:

HA Granules (Hydroxyapatite): HA granules, with a diameter range of 600 μm to 1.0 mm and a porosity of approximately 70 % with 99 % connectivity, served as the primary scaffold material. These granules were specifically designed to provide mechanical strength and support cellular infiltration during bone regeneration.

TH Composite (β-TCP Microspheres and Hydrogel Mixture): The TH composite consisted of β-TCP microspheres, with diameters ranging from 45 to 75 μm and a porosity of about 68 %, combined with a hydrogel mixture made of Poloxamer 407 (BASF Canada Inc., British Columbia, Canada) and HPMC (Spectrum Chemicals and Laboratory Products, Gardena, CA). Poloxamer 407 is a biodegradable, non-toxic polymer known for its temperature-dependent thermal conformation, while HPMC helps maintain the hydrogel structure [34,37–39]. Together, these components in a 1:1 wt ratio promote the slow and sustained release of rhBMP-2, ensuring a controlled delivery within the BGM.

rhBMP-2 Preparation: Recombinant human bone morphogenetic protein-2 (rhBMP-2) used in this study was derived from *E. coli* (Daewoong pharmaceutical co. ltd, Republic of Korea.), and there was no significant difference in clinical indicators compared to CHO cell-derived rhBMP-2, a more commonly-used mammalian hydrogel [34, 37–39]. Also, both rhBMP-2s posed no side effects or abnormalities including wound infection and neurological symptoms [40–42]. The rhBMP-2 powder was provided in a lyophilized form to ensure stability and ease of handling.

WFI (Water for Injection): WFI ensures sterility and acts as a solvent for the preparation of rhBMP-2.

This carefully designed formulation was used in all subsequent in vitro and in vivo experiments, ensuring the controlled and sustained release of rhBMP-2 for effective bone regeneration.

2.3. In vitro assays

2.3.1. Enzyme-linked immunosorbent assay (ELISA)

ELISA was performed to confirm the rhBMP-2 release mode according to the composition ratio of HA and TH. BGM containing 4 μg of rhBMP-2 was used to fill the inserts of a six-well insert system (pore size = 0.4 μm; SPL Life Sciences, Pocheon, Korea) with HA and hydrogel ratios of 1:2 and 2:3. Phosphate-buffered saline (PBS, Hyclone, Logan, UT, USA) was used as a buffer to fill the well plate. The amount of rhBMP-2 secreted across the insert membrane was quantified at 12 h and 1, 2, 4, 7, 14, and 24 days. Quantitation was performed according to the prescribed procedure of the human BMP-2 ELISA kit (RHF913CKX, Antigenix America Inc., Melville, NY, USA). Measurements were obtained at 450 nm using a microplate reader (Synergy™ HTX Multi-Mode Microplate Reader, BioTek Instruments, Winooski, VT, USA).

2.3.2. Cell culture

After obtaining rat neck adipose tissue, the cells were reacted with 0.2 % type I collagenase (in Hanks' balanced salt solution) in a water bath at 37 °C for 60 min, neutralized with 10 % fetal bovine serum (FBS)/Dulbecco's Modified Eagle Medium (DMEM), and sorted through a 70-μm cell strainer. Red blood cells were lysed with ammonium chloride potassium lysing buffer for 3 min and centrifuged at 800 g for 10 min at 4 °C to obtain SVF pellets. SVF pellets were then resuspended in DMEM supplemented with 10 % FBS and 1 % P/S medium and subcultured [43,44]. Isolated rat adipose tissue-derived SVF (rSVF cells) cells were used in vitro experiments.

hMSCs derived from adipose stem cells (R7788115; Invitrogen, Carlsbad, CA, USA) were seeded in a culture plate with a MesenPRO RS™ Medium kit (12746012; Gibco, Grand Island, NY, USA) and cultured in a humidified environment with 5 % CO2 at 37 °C.

The two cell lines were seeded in six-well plates (6.3×10^3 cells/cm^2) individually or jointly. Additionally, to confirm the effect of rhBMP-2 on the cells, BGM was added to the Transwell to induce the sequential release of rhBMP-2. The medium was changed two times per week for 3 weeks.

2.3.3. Osteodifferentiation

To analyze the osteogenic potential of composites, cells, and rhBMP-2, hMSCs and rSVF cells were seeded (5×10^3 cells/cm^2) in 24-well plates. BGM was added to the insert system during ELISA, and the cells were allowed to differentiate for 1–3 weeks. The range of 1–3 weeks was chosen to capture different stages of osteodifferentiation and observe both early and late markers of osteogenesis. Osteogenic differentiation is a gradual process, and evaluating multiple time points helps provide a more comprehensive understanding of how the composites, cells, and rhBMP-2 influence differentiation over time. By examining intervals within this range, we can identify temporal patterns in marker expression and activity, which may not be apparent if only a single endpoint were selected.

For the alkaline phosphate (ALP) activity assay, cells were harvested, washed with PBS (Hyclone), and resuspended in assay buffer. The cells were homogenized rapidly and centrifuged for 3 min at 4 °C at 13,000 g. The supernatant was collected, transferred to a new tube, and dispensed into a well plate. MUP Reaction Mix (MUP substrate + assay buffer), was added, and the samples were protected from light and incubated for 30 min at 25 °C. After adding Stop Solution, the samples were shaken gently and measured using a fluorometric microplate reader (VARIOSKAN LUX, Thermo Fisher Scientific Inc., Waltham, MA, USA) at excitation/emission wavelengths of 360/440 nm. All experiments were performed using the included reagents according to the protocol provided in the Alkaline Phosphatase Assay Kit (ab83371, abcam, Cambridge, MA, USA).

For Alizarin red staining, cells were washed with 1X DPBS (Hyclone) and fixed with 10 % formalin for 20 min. After fixation, the cells were washed three times with DPBS for 3 min. Then, the cells were stained with 2 % Alizarin Red S solution (Sigma-Aldrich, St Louis, MO, USA) for 5–30 min and washed three times with distilled water for 3 min. The cells were dried for 1–2 days to remove moisture at room temperature.

Expression of Runt-related transcription factor 2 (RUNX2, ab76956, 1:100, abcam) and osteocalcin (OCN, ab13418, 1:100, abcam) was confirmed by immunocytochemical staining.

2.3.4. Angiogenesis and tubule formation assay

hMSCs and rSVF cells were plated and seeded (5×10^3 cells/cm^2) individually or jointly in 24-well plates coated with Matrigel (356234, Corning, NY, USA). The cells were incubated in the appropriate medium for 1 day, and the medium was replaced with EGM™-2 basal medium (CC-3156, Lonza, Allendale, NJ, USA) and EGM™-2 singleQuots® supplements (CC-4176, Lonza) medium the next day. After 1 week in culture, the cells were stained with a CD31 antibody (ab124432, 1:400; abcam) for confirmation, and after 2 weeks in culture, they were stained with 2 μg/ml calcein AM (Thermo Fisher Scientific Inc.) to measure branch points and total tube length.

2.3.5. Quantitative reverse transcription-polymerase chain reaction (RT-qPCR)

The total RNA from the sample was isolated using TRIzol reagent (Thermo Fisher Scientific Inc.), following the manufacturer's instructions. The RNA pellet was resuspended, and the RNA concentration was determined. The RNA from each sample was reverse-transcribed using amfiRivert cDNA Synthesis Platinum Master Mix (GenDEPOT, Barker, TX, USA) in duplicate. PCR was performed using Power SYBR® Green PCR Master Mix (Thermo Fisher Scientific Inc.) with a QuantStudio 3 real-time PCR instrument (Applied Biosystems, Foster City, CA, USA). The PCR conditions were as follows: 50 °C for 2 min; 95 °C for 3 min; 40 cycles of 95 °C for 5 s, 60 °C for 30 s, and 95 °C for 15 s; and 60 °C for 1 min. The following primers were used: CD31 F: 5′CTGAGGAAAGCCAAGGCCAAG3′ and R: 5′TGTTGGAGTTCAGAAGTGG3′; VEGF-A F: 5′ACTGGACCCT GGCTTTACTG3′ and R: 5′CTGCTCCCCTTCTGTCGT3′; Angiophoietin-1 F: 5′ATGCGCCCTTATGCTAACAG3′ and R: 5′TTTAGATTGGAAGGGCCAC A3'; and GAPDH F: 5′TGCACCACCAACTGCTTAGC3′ and R: 5′AGGGGCC ATCCACAGTCTTC3'. GAPDH was employed as an internal control. The $2^{\Delta\Delta Ct}$ method was used to analyze the relative expression of genes.

2.3.6. Immunocytochemistry

The cells were fixed in a 4 % paraformaldehyde solution for 10 min, washed, and permeabilized carefully with 0.3 % Tween 20 (Sigma-Aldrich) in PBS solution. The cells were then blocked with 10 % normal donkey serum in 0.3 % Triton X-100 (Sigma-Aldrich) for 1 h to reduce the nonspecific background noise. The blocked cells were incubated overnight at 4 °C with primary antibodies diluted in the blocking solution. Then, the samples were washed three times with 0.3 % Tween 20 in PBS and treated with species-specific secondary antibodies for 1 h at room temperature. After antibody labeling, the cells were washed with 0.3 % Tween 20 in PBS, and nuclei were stained with a mounting solution containing DAPI (Vector Laboratories, Inc., Burlingame, CA, USA). Fluorescent images were captured using a confocal laser microscope (LSM700; Carl Zeiss, Oberkochen, Germany).

2.4. In vivo studies: surgical techniques and post-operative analyses

2.4.1. Preparation of human adipose tissue-derived SVF cells for animal transplantation

hSVF (human adipose tissue derived SVF) cells used for in vivo studies were isolated with an automatic hSVF extraction device (Cellunit, CGBio Co.). The adipose tissue used in the experiment was collected from the abdominal fat of women aged 39–60 years, refrigerated at 4 °C immediately after collection, and used within 24 h. SVF cells were harvested using the Cellunit and prepared by diluting 1.5×10^5 cells for posterolateral fusion (PLF) and 5×10^6 cells for OLIF in 100 µl of PBS (Hyclone). Only cells that passed serology evaluation were used. Furthermore, all experiments were performed according to established protocols, with the consent of all patients, and in accordance with established standards of the Severance Hospital Institutional Review Board (approval number: 4-2020-1121).

2.4.2. Rat PLF model

In this study, 48 male Sprague-Dawley rats (200 ± 10 g) were divided into four groups, and PLF was performed bilaterally at lumbar level 4–5. All animal care and surgeries were performed in accordance with Association for Assessment and Accreditation of Laboratory Animal Care (AAALAC) regulations and were managed and supervised with Institutional Animal Care and Use Committee (IACUC; protocol number: 2020-0326) approval. Rats were anesthetized with a general anesthetic (100 mg/kg; ketamine, Yuhan, Seoul, Korea) and a muscle relaxant (10 mg/kg; Rompun, Bayer, Leverkusen, Germany) via intraperitoneal injection, followed by administration of a respiratory anesthetic (Isotroy 100, Troikaa Pharmaceuticals Ltd, Gujarat, India) to maintain anesthesia. Rats were fixed in a prone position, and muscle and bone were separated at lumbar level 4–5 based on the position of the iliac bone. The

surface of the neural arch between the mammillary and transverse processes was decorticated using an electric drill or scalpel to remove the cortical bone and expose the cancellous bone. Initially, hSVF cells (1.5×10^5 cells/100 µl) were spread in the target region, and BGM (rhBMP-2, 0.4 mg/cm^3) was transplanted. Then, the muscle was sutured, and antibiotics were administered (5 mg/kg; cefazoline, Chong Kun Dang Pharmaceutical Corporation, Seoul, Korea) for 1 week [45,46] (Fig. 2A). After 8 weeks, lumbar spine samples were obtained for imaging and mechanical/histological analysis. The four experimental groups were as follows: 1. HA/TH (Ctrl), 2. HA/TH/1 µg rhBMP-2 (rhBMP-2), 3. HA/TH with SVF (SVF), 4. HA/TH/1 µg rhBMP-2 with SVF (rhBMP-2 + SVF).

2.4.3. Biomechanical bending tests for PLF samples from rats

Eight weeks after PLF, we obtained lumbar level 3–6 spinal tissue containing fusion regions from rats. A three-point bending test was performed [45–47] on the collected samples using a Universal Testing Machine (TO-101, Testone, Seoul, Republic of Korea). The vertebral body of the sample was placed in contact with the two support pins, with the spinous process facing upward. The distance between the lower supporting pins was 10 mm, and the loading pin was positioned in the middle of the sample. The three-point bending test was performed at 50 mm/min until the upper loading pin advanced to 15 mm (Fig. 2B). The force-displacement curve of this test helps identify the flexural strength, which represents the highest stress experienced by the sample at the moment it ruptures. The flexural load and deflection curve were used to calculate the flexural modulus.

2.4.4. Minipig OLIF model

In this study, a total of 15 minipigs (*Sus scrofa domestica*, 50 ± 5 kg, female, mean ± standard deviation; CRONEX M-Pig®, CRONEX Co., Ltd, Korea) were divided into three groups, and OLIF were performed at 2 non-continuous of levels (at L2-L3 and L4-L5) vertebral bodies on each of animal (Fig. 5A). Surgery and breeding were managed and supervised according to a protocol approved by the IACUC (protocol number: 2019-0061) in accordance with AAALAC regulations, similar to the small animal experiments. Minipigs were anesthetized with anesthetics (100 mg/kg; ketamine, Yuhan), muscle relaxants (10 mg/kg; Rompun, Bayer), and respiratory anesthetics (Isotropy 100, Troikaa Pharmaceuticals Ltd.). The minipigs were fixed in the lateral position, and the target level was confirmed by c-arm imaging. Muscles were separated until the vertebral body of the targeted spinal segment appeared, and the space was secured to drive the screw into the disc space. Careful attention was required because contacting the spinal nerve would result in paralysis. Once the target level was reached, the intervertebral disc (or intervertebral fibrocartilage) was removed between lumbar levels 2–3 and 4–5, and the exposed end plate of the vertebral body was further drilled and scraped. hSVF cells (5×10^6 cells/100 µl) were first applied to the disc space. Then, the polyetheretherketone (PEEK) cage (CGBio co.,Ltd.) was filled with BGM (rhBMP-2, 0.4 mg/cm^3) and transplanted into the interbody space. Autologous bone was obtained from the iliac bone of animals, and bone chips (3–4 mm) were filled into PEEK cages, mainly on cancellous bones without cortical bones. To increase the fusion rate, a screw (G.S. Medical, Chungcheongbuk-do, Korea) was driven into the vertebral body and fixed with a rod (G.S. Medical) (Fig. 5A). Animals were given antibiotics (15 mg/kg; cefazoline, Chong Kun Dang Pharmaceutical Corporation) and the anti-inflammatory pain reliever meloxicam (0.2 mg/kg; Metacam; Boehringer Ingelheim, Barcelona, Spain) for 1 week, and the lumbar spines were obtained at 8 and 16 weeks for imaging, mechanical, and histological analyses [32]. The three experimental groups were as follows: 1. Autologous bone graft; ABG, (N = 10), 2. Novosis Putty (276 µg rhBMP-2/Level), (N = 10), 3. Novosis Putty (276 µg rhBMP-2/Level) with hSVF, (N = 10).

2.4.5. Spinal kinematics test for OLIF samples from minipigs

The rod was removed from all minipig spine samples obtained at 8

and 16 weeks, and lumbar vertebral levels 2–5 were isolated to confirm the effects of the implanted material and elapsed time on fusion. Lateral bending is the measured value of bending to both sides relative to the center line in the coronal plane, and flexion-extension is the measured value of bending back and forth in the coronal plane. Lateral bending and flexion-extension were measured using a three-point scale: 3 points when moving freely and 0 points when not moving at all (Fig. 5B).

2.4.6. Micro-computed tomography (CT)

After sacrificing the rats at 8 weeks and minipigs at 8 and 16 weeks by exsanguination, the fusion site was isolated and fixed in 10 % formalin solution at room temperature for 7 days. The spine samples were scanned using a Skyscan1173 micro-CT imager (Bruker-CT, Kontich, Belgium) and image-controlling software (version 1.6, SkyScan 1173, Bruker-CT). Scanning was performed on 2240 slides with an energy of 130 kVp, a current of 60 μA, and a voxel size of 7.1 μm. Three-dimensional (3D) reconstruction of the raw image data was performed using CTVOX (Ver. 3.3.0, Bruker-CT). Reconstructed images were analyzed using CTAn Software (Ver. 1.19.40., Bruker-CT). We performed fusion and heterotopic ossification formation analysis using 2D images, and cancellous bone analysis was performed using 3D images. In 3D images, analysis was performed separately for whole and new bone, and various comparative analyses of cancellous bone were performed by group.

2.4.7. Histological staining and analysis

2.4.7.1. Sample preparation for staining.
Specialized staining procedures, such as Hematoxylin and eosin (HE), Goldner's trichrome (GT), and Von Kossa (VK) staining, require a pretreatment step to ensure proper preservation and staining of the undecalcified tissue. First, the tissue was dehydrated by immersion in 70 % ethanol (Sigma-Aldrich) for 2 days, 95 % ethanol for 2 days, and 100 % ethanol for 3 days. The samples were then embedded for 3 days in Technovit 7200 (VLC, Heraeus Kulzer, Wehrheim, Germany), a light-curing methacrylate-based resin component. The samples were carefully polymerized using a photopolymerization apparatus (Exact 520, Exact, Norderstedt, Germany) so that the temperature would not exceed 40 °C. The embedded sample was cut to a specific size, prioritizing the fusion site, and then attached to an acrylic slide. Samples were then cut to a thickness of approximately 300 μm using a cutting band (Exakt 300, Exact) and re-polished to 60 μm with the same machine and sandpaper before staining.

2.4.7.2. Hematoxylin and eosin (HE) staining.
Samples were stained with Mayer's hematoxylin (Sigma-Aldrich) for 10 min and washed with tap water for 10 min. After staining with 1 % alcohol and Eosin Y (Sigma-Aldrich) for 10 s, the samples were dehydrated twice each in 70 %, 95 %, and 100 % ethanol. Then, the slides were mounted using a permanent mounting medium (Permount™ Mounting Medium, Electron Microscopy Sciences, Hatfield, PA, USA).

In HE staining of OLIF tissue, the total area was measured after photographing to include the rectangular area inside the cage, and the interest rate occupied by new bones and transplants in the rectangular area was measured, respectively. Soft tissue was calculated as the remaining area excluding new bones and transplant material from the total area.

2.4.7.3. Goldner's trichrome (GT) staining.
Samples were stained with Weigert's iron hematoxylin (Sigma-Aldrich) for 5 min and washed with tap water for 10 min. Then, the slide was stained blue with a ponceau acid fuchsine solution (Sigma-Aldrich) for 5 min, followed by washing with 1 % acetic acid (Sigma-Aldrich) for 1 min. Samples were treated with Orange G solution (Sigma-Aldrich) for approximately 5 min until collagen decolorization and washed again with 1 % acetate (Sigma-

Aldrich) for 1 min. Finally, the samples were treated with a light green solution (Histo-Line Laboratories, Pantigliate, Milano, Italy) for 10 min, followed by extensive washing with tap water. The samples were sequentially dehydrated with 70 %, 95 %, and 100 % ethanol and mounted using Permount™ Mounting Medium (Electron Microscopy Science).

2.4.7.4. Von Kossa (VK) staining.
Before staining, the samples were hydrated with distilled water and reacted in a 10 % silver solution (Sigma-Aldrich) in an oven at 70 °C for 20 min. Then, one to three drops of 10 % silver solution were applied, and the samples were incubated in EXAKT 520 (Gen-R-103, Exact) for approximately 30 min until the Ca^{2+} in the sample turned black. After washing with tap water and rinsing with distilled water, one to three drops of 5 % sodium thiosulfate (Sigma-Aldrich) was added dropwise and allowed to react for 3 min. After washing with tap water and rinsing with distilled water, one to three drops of nuclear fast red (Sigma-Aldrich) were added, and then the samples were washed with tap water. Finally, after dehydration with 70 %, 95 %, and 100 % ethanol, the samples were mounted using Permount™ Mounting Medium (Electron Microscopy Science).

2.4.7.5. Slide scanning and image analysis.
All stained slides were scanned using an automated digital slide scanning system (Pannoramic 250 FLASH III, 3D HISTECH, Sysmex, Budapest, Hungary), and the obtained images were processed using CaseViewer (3D HISTECH, Sysmex).

2.5. Statistical analysis

All data are presented as the mean ± standard error of the mean (SEM). One-way and Two-way ANOVA were performed to compare the groups, followed by Tukey's post-hoc test for multiple comparisons when significant differences were found (*, $p < 0.05$; **, $p < 0.01$; and ***, $p < 0.001$). The assumptions of normality and homogeneity of variances were tested prior to ANOVA. A p-value of <0.05 was considered statistically significant. GraphPad PRISM 10.2.0 (GraphPad Software Inc., CA, USA) was utilized for all graphing and statistical analyses.

3. Results

3.1. Confirmation of the release pattern of rhBMP-2 according to ceramic composition, and osteodifferentiation effect by rhBMP-2 and rSVF

BGM (bone graft materials) is a complex of HA and TH that can modulate the release rate of rhBMP-2 and the cellular response, depending on the composition ratio of the two carriers [48,49]. Previous studies have suggested that the release kinetics of HA + β-TCP are attributable to their particle sizes. Specifically, HA has a large particle size and dissolves slowly, whereas β-TCP has a small particle size and is quickly absorbed [32,34]. In a previous study, we confirmed that using a mixture of HA and TH was more appropriate for the low-speed emission of rhBMP-2 than using a mixture of HA and TH, and the mixing ratio of these two materials was 1:2 [32]. In this study, the ratio of the two materials was changed to 2:3, resulting in the release of a lower amount of rhBMP-2 (1405.25 ± 18.62 ng/mL) on days 0–4 compared to the 1:2 ratio (1826.88 ± 5.18 ng/mL). Conversely, a sustained release of a higher amount of rhBMP-2 was observed until week 3 (615.6 ± 198.7 ng/mL for the 2:3 ratio compared to 245.95 ± 105.37 ng/mL for the 1:2 ratio) (Fig. 1A–C). These results indicate that the use of HA + TH in a ratio of 2:3 is more ideal for the sustained release of low-dose rhBMP-2.

rSVF, known to include FBs, MSCs, and ECs, as well as smooth muscle cells, mural cells, macrophages, and other immune cells, was used in vitro studies [50]. Therefore, angiogenesis and vascularization by various cells and factors contained in rSVF can be expected to have a positive effect on bone fusion [51,52]. A 6-well insert system was used to confirm the osteodifferentiation effect of low dose sustained release
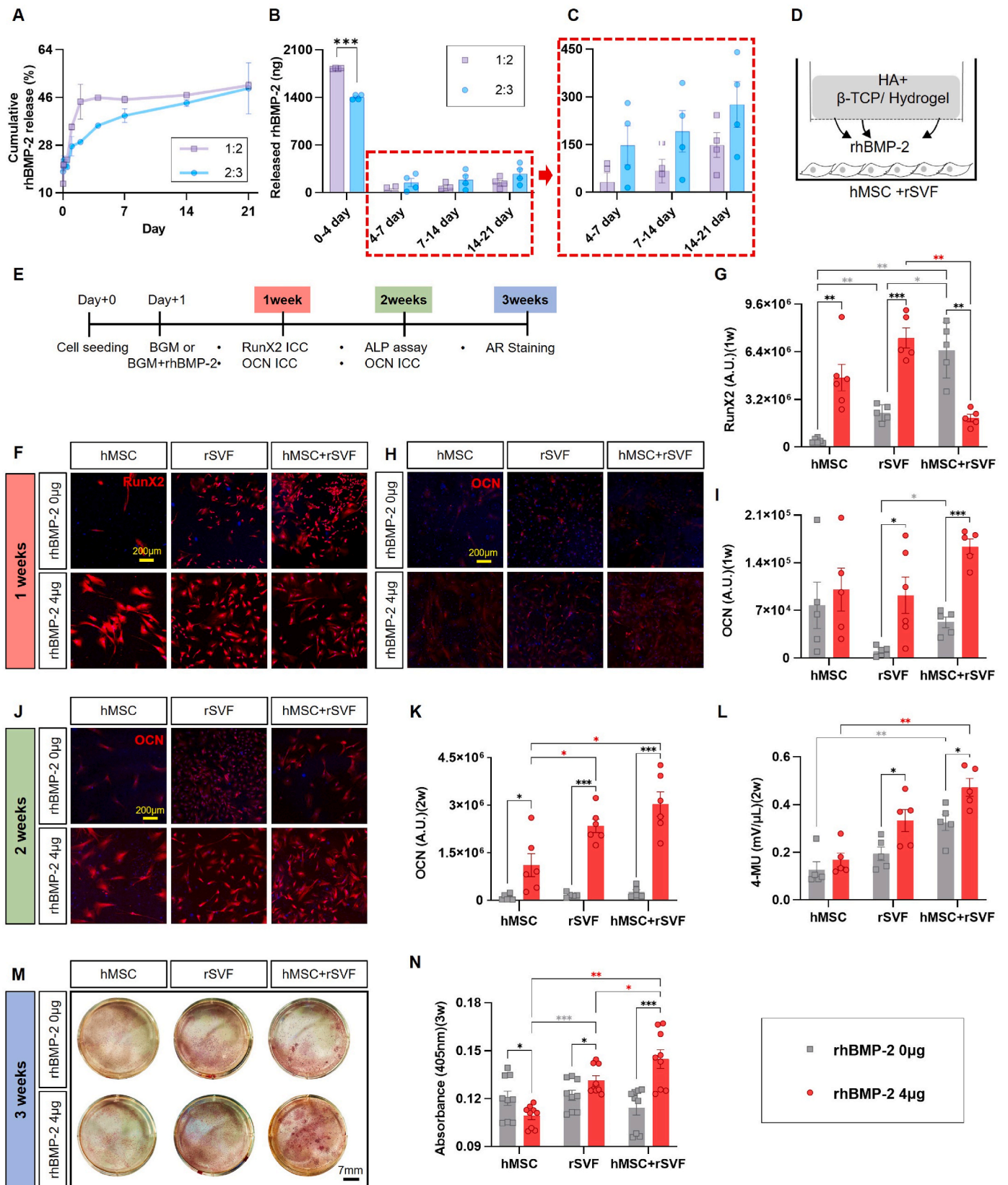
(caption on next page)

Fig. 1. Osteogenic ability of hMSCs and rSVF cells according to the rhBMP-2 concentration *in vitro*.
A) *In vitro* release kinetics of rhBMP-2 depending on carrier composition ratio. B) Amount of rhBMP-2 released at 0–4, 4–7, 7–14, and 14–21 days depending on carrier composition ratio. BGM ratio of 2:3 provided a more sustained rhBMP-2 release than 1:2. C) A closer inspection of amount of rhBMP-2 released. D) Schematic illustration of BGM releasing rhBMP-2 with hMSCs and rSVF cells. E) Experimental osteogenic differentiation timeline. F) Confocal imaging of hMSC, rSVF, and hMSC + rSVF cell groups to visualize osteodifferentiation at 1 week with anti-RunX2 (red) and DAPI (blue). rhBMP-2 concentrations were 0 and 4 μg, respectively. G) Mean intensity of RunX2 in each group. H) Confocal imaging of hMSC, rSVF, and hMSC + rSVF cell groups to visualize osteodifferentiation at 1 week using anti-OCN (red) and DAPI (blue). The rhBMP-2 concentrations were 0 and 4 μg, respectively. I) Mean intensity of OCN in each group. J) Confocal imaging of hMSC, rSVF, and hMSC + rSVF cell groups to visualize osteodifferentiation at 2 weeks using anti-OCN (red) and DAPI (blue). The rhBMP-2 concentrations were 0 and 4 μg, respectively. K) Mean intensity of OCN in each group. L) Comparison of ALP activity among all cell groups for two rhBMP-2 concentrations. M) Comparison of Alizarin red staining among hMSC, rSVF, and hMSC + rSVF cell groups for two rhBMP-2 concentrations. N) Alizarin red quantification by acid extraction at an absorbance of 405 nm *p* < 0.05, **p* < 0.01, and ***p* < 0.001 indicate statistically significant differences.
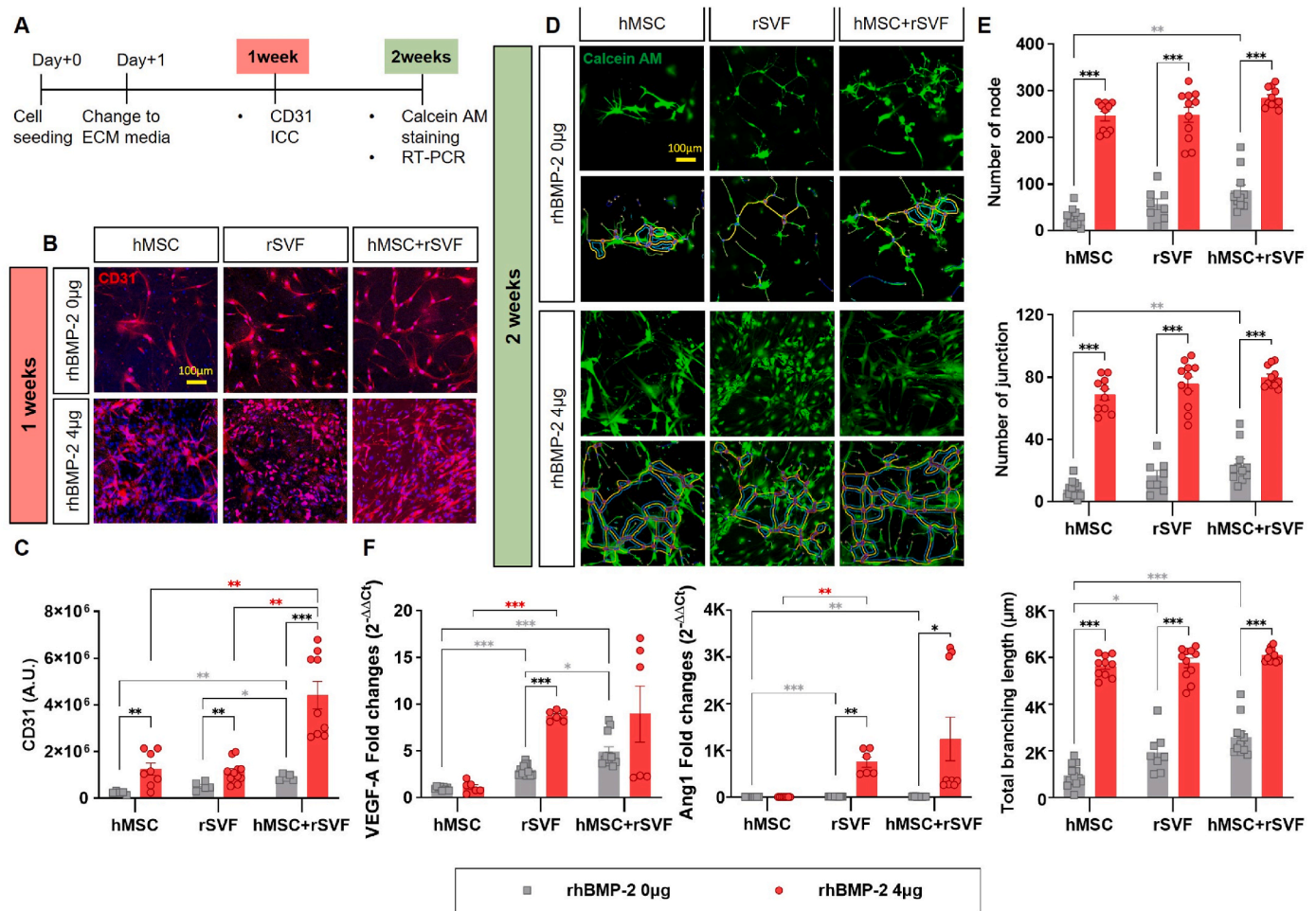

Fig. 2. The angiogenic ability of hMSCs and rSVF cells according to the rhBMP-2 concentration *in vitro*.
A) Experimental angiogenesis timeline of the hMSC, rSVF, and hMSC + rSVF groups. B) Confocal imaging of hMSC, rSVF, and hMSC + rSVF cell groups to visualize angiogenesis at 1 week using anti-CD31 antibodies (red) and DAPI (blue). The rhBMP-2 concentrations were 0 μg and 4 μg, respectively. The imaging shows that at 0 μg, there is limited CD31 expression across all groups. However, at 4 μg of rhBMP-2, an increased CD31 signal is observed, particularly in the hMSC + rSVF group, indicating enhanced angiogenesis. C) Mean intensity of CD31 in each cell group. The analysis indicates a significant increase in CD31 intensity in the hMSC + rSVF group at 4 μg rhBMP-2 compared to 0 μg, suggesting that higher concentrations of rhBMP-2 enhance angiogenic marker expression. D) Confocal imaging of hMSC, rSVF, and hMSC + rSVF cell groups to visualize vascularization at 2 weeks using calcein AM (green). At 4 μg rhBMP-2, there is more extensive network formation in the hMSC + rSVF group, demonstrating improved vascularization compared to the 0 μg condition. E) Quantification of angiogenesis using ImageJ software. The number of nodes and junctions, as well as the total branching length, were analyzed. Quantification shows a statistically significant increase in all three metrics for the hMSC + rSVF group at 4 μg rhBMP-2 compared to 0 μg, reflecting enhanced angiogenic capacity. F) Expression of angiogenesis markers, including CD31, VEGF-A, and Ang1, in the hMSC, rSVF, and hMSC + rSVF cell groups, analyzed by RT-qPCR. At 4 μg rhBMP-2, there is a significant upregulation of these markers in the hMSC + rSVF group compared to 0 μg, indicating that higher concentrations of rhBMP-2 stimulate the expression of angiogenic factors. *p* < 0.05, **p* < 0.01, and ***p* < 0.001 indicate statistically significant differences.

rhBMP-2 and rSVF cells (Fig. 1D). To confirm differentiation at each stage, immunofluorescence staining, and alkaline phosphate (ALP) activity assay, and Alizarin red staining were performed after inducing differentiation for 1, 2, and 3 weeks (Fig. 1E). At week 1, expression of RunX2, an early differentiation marker, was highest in the hMSC + rSVF group when rhBMP-2 was not applied and highest in the rSVF group when 4 μg of rhBMP-2 was applied. However, OCN, a more mature differentiation marker than RunX2, was most highly expressed in the hMSC + rSVF group when 4 μg of rhBMP-2 was released (Fig. 1F–I). At 2 weeks, ALP assay showed higher ALP expression in the hMSC + rSVF

group than in the hMSC or rSVF alone groups, but the results were not significantly affected by the presence or absence of rhBMP-2. However, OCN was also expressed most in the hMSC + rSVF group at week 2 and increased more than 20-fold compared with that at 1 week (Figure J–L). Finally, Alizarin red staining of areas containing Ca^{2+} at week 3 was largely unaffected by the presence of rhBMP-2 in single-cell cultures, whereas addition of 4 μg of rhBMP-2 to hMSC + rSVF co-cultures resulted in an increase in areas exhibiting Ca^{2+} (Fig. 1M and N).

These results suggest that hMSC and rSVF cells have complete osteogenic potential under favorable microenvironmental conditions in which osteodifferentiation is induced, and their differentiation ability is further enhanced when cultured together than when cultured individually.

3.2. Assessment of angiogenic effects of SVF through cellular and molecular analysis in vitro

Various studies have shown that human mesenchymal stem cells (hMSCs) possess intrinsic angiogenic potential [53,54]. As previously mentioned, SVF is a heterogeneous collection of cells that significantly influences the microenvironment. In particular, SVF exhibits notable angiogenic effect [55–58], largely due to its high content of FBs and endothelial cells, which synergize to enhance bone fusion. The angiogenic potential of hMSC, rat SVF (rSVF), and hMSC + rSVF groups was assessed at 1 and 2 weeks in vitro (Fig. 2A). The experimental timeline involved the application of rhBMP-2 at concentrations of 0 μg and 4 μg. Confocal imaging at 1 week, using anti-CD31 antibodies (red) and DAPI (blue), revealed limited CD31 expression across all groups at 0 μg of rhBMP-2 (mean fluorescence intensity: $238470 \pm 32186 \pm 78711$, 516203 ± 59591). However, at 4 μg of rhBMP-2, a significant increase in CD31 expression was observed, particularly in the hMSC + rSVF group (mean fluorescence intensity: 4415124 ± 595005) compared to the hMSC group alone (mean fluorescence intensity: 1246406 ± 258152) and the rSVF group alone (mean fluorescence intensity: 1124046 ± 141765). These findings indicate enhanced angiogenesis in the hMSC + rSVF group in response to 4 μg of rhBMP-2 (Fig. 2B). Quantitative analysis of CD31 intensity showed a statistically significant increase in the hMSC + rSVF group at 4 μg rhBMP-2 compared to 0 μg (Fig. 2C), suggesting that higher concentrations of rhBMP-2 amplify angiogenic marker expression. At 2 weeks, further confocal imaging with calcein AM (green) demonstrated more extensive vascular network formation in the hMSC + rSVF group at 4 μg rhBMP-2, compared to the 0 μg condition, illustrating improved vascularization (Fig. 2D). Quantitative measurements of angiogenesis, including the number of nodes, junctions, and total branching length, showed a significant increase in all three metrics for the hMSC + rSVF group at 4 μg rhBMP-2 (Fig. 2E). RT-qPCR analysis of angiogenesis markers such as CD31, VEGF-A, and Angiopoietin-1 (Ang1) further confirmed that higher concentrations of rhBMP-2 significantly upregulate these markers in the hMSC + rSVF group compared to 0 μg (Fig. 2F), indicating a robust enhancement of angiogenic capacity. Statistical significance was noted as *$p < 0.05$, **$p < 0.01$, and ***$p < 0.001$.

These results demonstrate that rSVF and hMSC have intrinsic angiogenic potential, suggesting that transplanting both cells together can have a stronger angiogenic synergistic effect on the recipient than single-cell transplantation.

3.3. Evaluation of spinal fusion and bone quality through biomechanical and Micro-CT analysis in the rat PLF model

We confirmed that hSVF cell transplantation and low-concentration rhBMP-2 sustained release can induce effective osteodifferentiation and angiogenesis in vitro. Therefore, we sought to validate these effects in an in vivo setting using a rat PLF model. First, we implanted the bone graft materials (BGM) into the lumbar spine of SD rats in the PLF model (Fig. 3A). After 8 weeks, the lumbar spines were harvested for further

analysis. Flexural strength, which refers to the maximum stress that the specimen can withstand before breaking, was measured to assess the material's ability to resist bending forces (Fig. 3B). Flexural strength was highest in the rhBMP-2 group among all groups (Fig. 3C and D). The flexural modulus, indicative of the material's stiffness and resistance to bending, was significantly greater in the rhBMP-2 and rhBMP-2 + SVF groups (Fig. 3C–E). In contrast, the SVF group showed varied results, with some samples exhibiting higher values than the Control group but with noticeable variability. The combination of rhBMP-2 + SVF minimized these inter-individual differences, suggesting a synergistic effect when both agents were applied together.

Micro-CT analysis provided detailed insights into the fusion mass. Axial 2D micro-CT images and coronal 3D-reconstructed images revealed the extent to which the implanted ceramic carrier was resorbed and integrated with the rat spine (Fig. 3F). In the Control group, the carrier did not fuse effectively with the spine, resulting in low bone density. The rhBMP-2 group exhibited better fusion, with increased bone density and integration between the carrier and the spine. The SVF group also demonstrated enhanced fusion compared to the Control, though less pronounced than the rhBMP-2 group. Notably, the rhBMP-2 + SVF group showed the highest bone density and the most effective fusion, underscoring the combined effects of these two agents.

The Cancellous bone consists of a trabecula network and has a porous structure and a wide surface, so It is involved in initial bone fusion for new bone formation [59,60]. Cancellous bone analysis was conducted using micro-CT images (Fig. 3G). In the rhBMP-2 group, the increase in cancellous bone was primarily due to thicker and more separated trabeculae. Conversely, the SVF group showed an increase in the number of trabeculae rather than their thickness. The rhBMP-2 + SVF combination resulted in both an increase in bone thickness and number, leading to significantly improved cancellous bone quality and quantity (Fig. 3H). This effect was not limited to the transplanted bone but also extended to the surrounding native bone, further confirming the synergistic effect of rhBMP-2 and SVF in enhancing bone fusion.

The osteodifferentiation and angiogenesis effects observed in the in vitro experiments were further supported by the in vivo outcomes in the PLF model. The combination of rhBMP-2 and SVF not only enhanced bone fusion but also improved the integration and quality of the newly formed bone, confirming the synergistic effects of these factors. These results indicate that the osteogenic and vascularization capabilities observed in vitro can be successfully translated into enhanced spinal fusion outcomes in vivo, highlighting the potential for clinical application of this combined treatment approach.

3.4. Histological analysis of bone formation and fusion mass in the rat PLF model

Histological analysis was performed on tissue samples collected 8 weeks post-fusion to evaluate the quality and extent of bone formation. Cross-sectional and longitudinal sections of the fusion site were analyzed using HE staining, GT staining, and VK staining (Fig. 4A). HE staining was used to confirm whole bone sites, highlighting general tissue morphology (pink and purple) and identifying any inflammatory reactions. GT staining differentiated mineralized bone (green) from osteoid bone (orange), which is important for assessing the stages of bone formation, and also helped to check for any inflammatory response. Finally, VK staining was employed to identify Ca^{2+}-positive sites (dark brown), providing insights into the degree of bone mineralization.

HE staining revealed the distribution of bone and implanted materials. In the BGM (Control) group, the bone formation area was minimal (0.1454 ± 0.02 mm^2). The SVF group showed a slight decrease in bone formation area (0.0648 ± 0.022 mm^2), suggesting limited osteogenic potential when SVF was used alone. In the rhBMP-2 group, bone formation was more pronounced (0.1692 ± 0.037 mm^2), indicating the osteoinductive effect of rhBMP-2. Notably, the combination of rhBMP-2
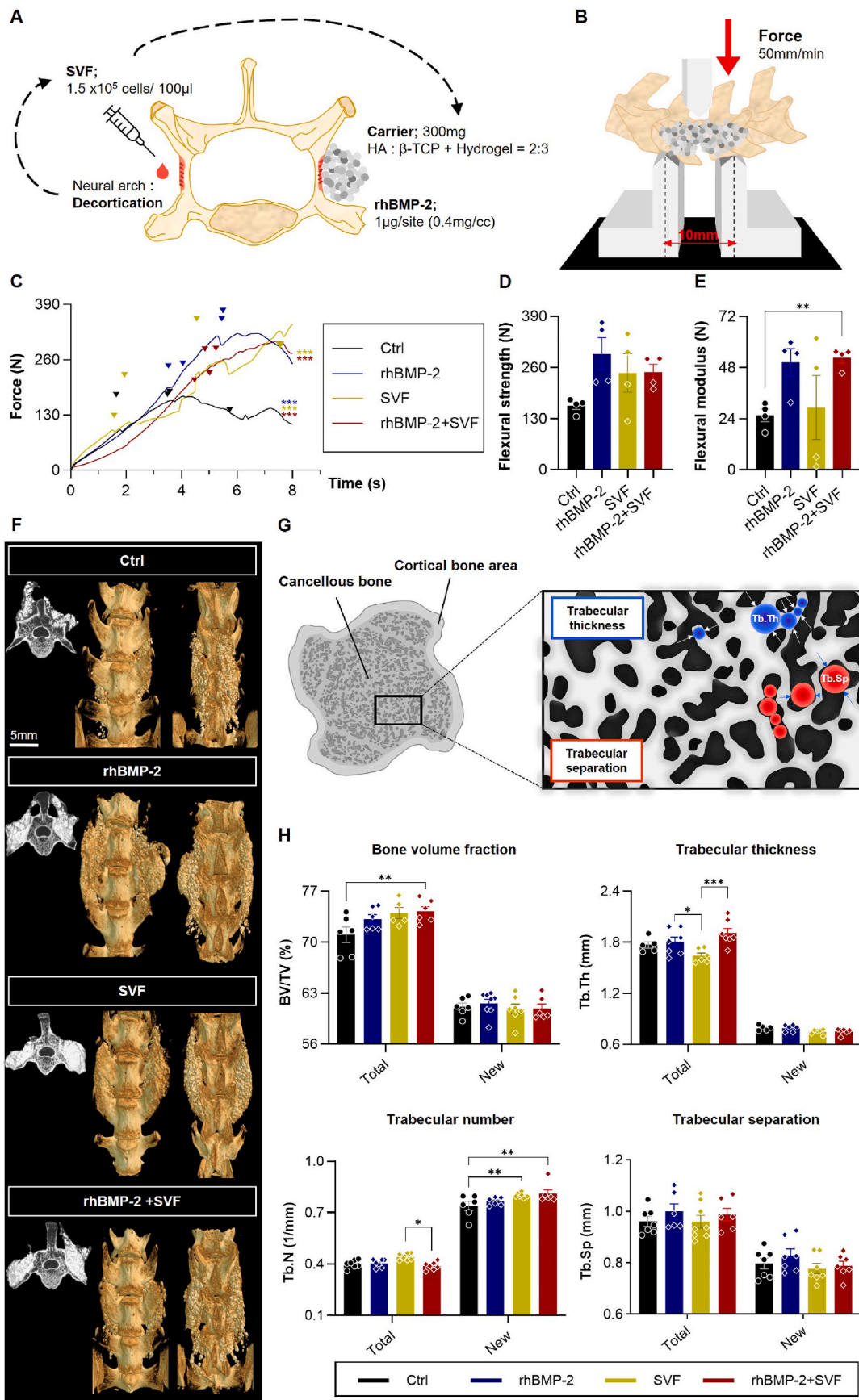
(caption on next page)

Fig. 3. Scaffold in the rat PLF model and biomechanical assessment at 8 weeks.

A) Schematic image of the hSVF and BGM transplantation conditions in the rat PLF model. B) Experimental design for the three-point bending test. The arrow indicates the direction and intensity of the force applied to the fusion area. C) Force-displacement graph of the fusion mass for each group and individual flexural strength data. D) Flexural strength data for each experimental group. The flexural strength indicates the strength required to break the fusion mass in each group. E) Flexural modulus data for each experimental group. The flexural modulus indicates the tension required to withstand an applied force in each group. rhBMP-2 increased bone strength, and hSVF cells decreased stiffness. As a result, the rhBMP-2 + SVF group had adequate strength and flexibility of the fused spine. F) Micro-CT image of the spinal fusion region for each experimental group, 2D and 3D reconstruction. G) Different analysis method of the cancellous bone in MicroCT images. H) Analysis of total and newly formed bone mass in the cancellous bone for each experimental group. rhBMP-2 increased trabecular thickness, and hSVF cells increased the trabecular number. Therefore, rhBMP-2 + SVF implantation increased the bone volume fraction. $*p < 0.05$, $**p < 0.01$, and $***p < 0.001$ indicate statistically significant differences.
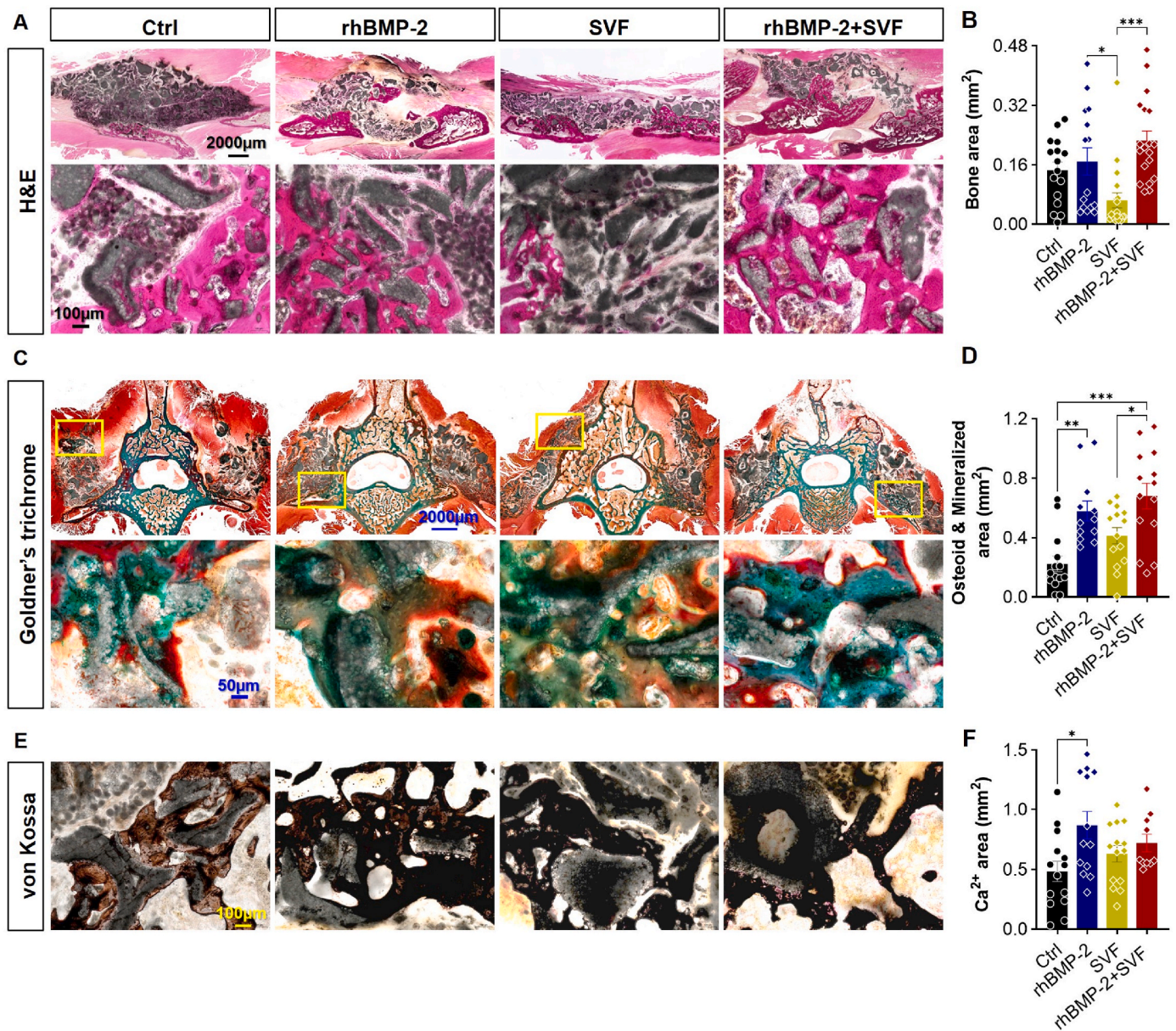

Fig. 4. Histological assessment of the fusion mass at 8 weeks after PLF.

A) HE staining showsing inflammatory reactions in the bone area for the four groups (pink and purple). B) Graph of bone area of the four groups. C) GT staining shows osteoid areas (red and orange) and mineralized areas (blue-green). D) Graph of osteoid and mineralized areas. E) VK staining shows Ca^{2+}-positive areas (dark brown). F) Graph of Ca^{2+}-positive areas. rhBMP-2 increased bone area and mineralized area associated with Ca^{2+} pathways that promote osteogenesis. hSVF cells had a greater effect on the mineralized area than on the osteoid area. Put together, the rhBMP-2 + SVF group showed the greatest increase in total bone area. All images consist of spine cross sections and sagittal sections; spine cross sections were quantified. $*p < 0.05$, $**p < 0.01$, and $***p < 0.001$ indicate statistically significant differences.
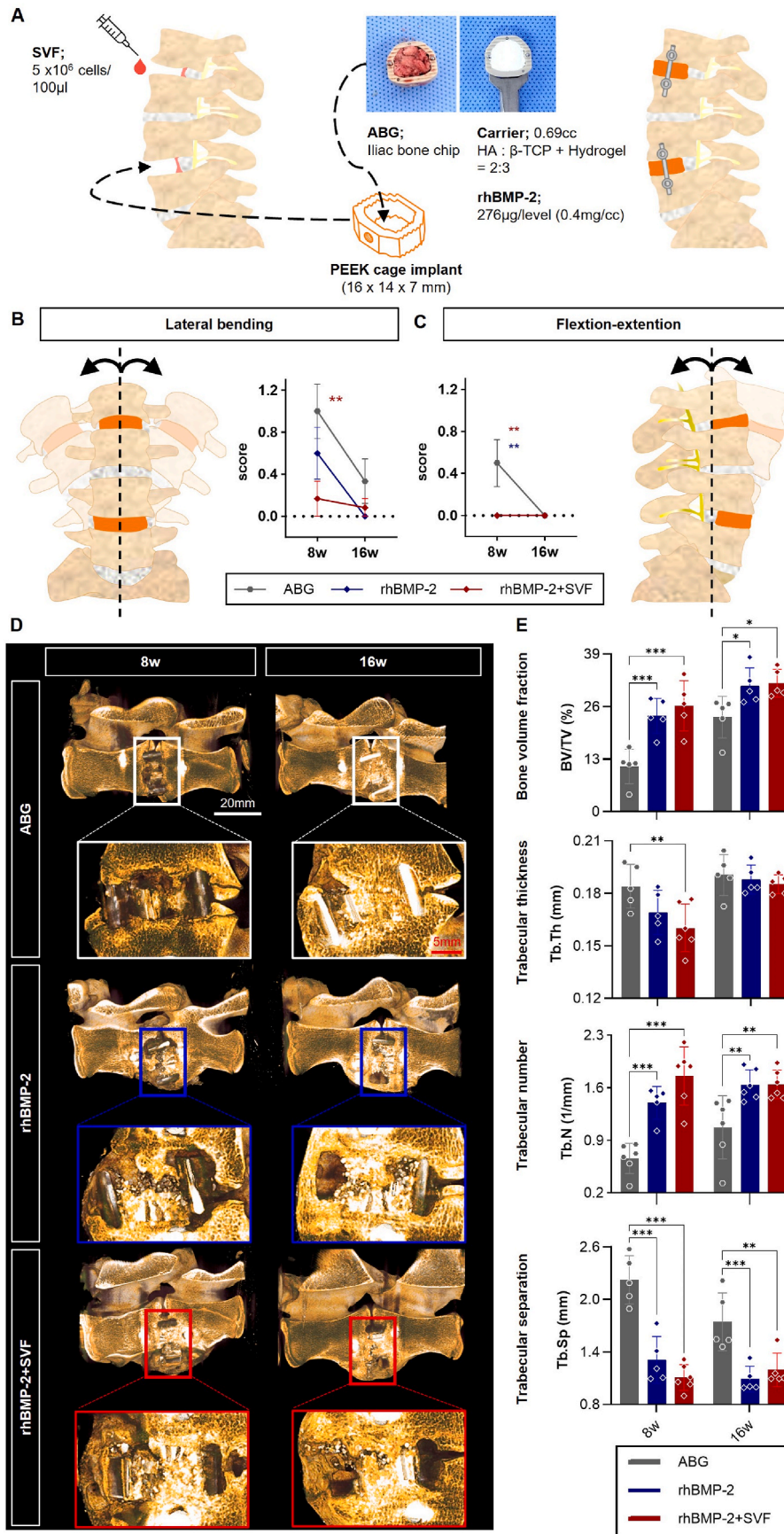
(caption on next page)

Fig. 5. BGM and SVF transplantation in the minipig OLIF model and kinematics test and Micro-CT analysis to confirm the fusion rate of the OLIF mass.
A) Schematic image of SVF and BGM transplantation conditions in the minipig OLIF model. After implanting hSVF cells at lumbar vertebral levels 2–3 and 4–5, BGM was placed inside a PEEK cage and implanted. B) Lateral bending test of fused bone at 8 and 16 weeks. C) Flexion-extension of fused bone at 8 and 16 weeks. Free movement in lateral bending and flexion-extension was recorded as 2 points, and no movement was recorded as 0 points. D) Micro-CT imaging of the fusion site centering on the 3D-reconstructed cage implantation site. E) Analysis of newly formed cancellous bone mass. Compared with the ABG group, rhBMP-2 and rhBMP-2 + SVF transplantation promoted the generation of new cancellous bone. In particular, the increase in the trabecular number caused the trabecular separation to decrease, increasing the total bone mass. Furthermore, during the last week of observation (week 16), the bone thickened to approximately the same thickness as the autologous iliac bone. $*p < 0.05$, $**p < 0.01$, and $***p < 0.001$ indicate statistically significant differences.

and SVF resulted in the most extensive bone formation (0.2256 ± 0.02567 mm^2), highlighting the synergistic effect of this combination. Importantly, no inflammatory response was observed across any group (Fig. 4A and B).

GT staining, which differentiates between mineralized bone (green) and osteoid bone (orange), provided additional insights into the bone formation process. In the Control group, the total bone area was the smallest (0.2233 ± 0.0531 mm^2), with limited mineralization. The SVF group demonstrated a moderate increase in total bone area (0.4129 ± 0.0549 mm^2), attributed primarily to the formation of osteoid bone. The rhBMP-2 group exhibited a significant enhancement in total bone area (0.5800 ± 0.0677 mm^2), indicating effective bone mineralization. Importantly, the combination of rhBMP-2 and SVF resulted in the highest total bone area (0.6804 ± 0.0862 mm^2), with a markedly larger mineralized bone area compared to other groups. These findings highlight that while rhBMP-2 serves as the primary driver of bone mineralization, SVF plays a complementary role by promoting osteoid bone formation, creating synergistic effects that lead to the most extensive and well-mineralized bone formation observed among all groups (Fig. 4C and D).

VK staining confirmed the presence of Ca^{2+}-positive areas within mineralized bone, with the rhBMP-2 group showing the greatest increase. However, there was no significant difference between the rhBMP-2 group and the rhBMP-2 + SVF group, suggesting that while rhBMP-2 is crucial for mineralization, the presence of SVF mainly enhances the osteoid phase and overall bone volume rather than just mineral content (Fig. 4E and F).

The histological analysis of the fusion mass further corroborated the findings from the in vitro experiments, demonstrating that the combined use of rhBMP-2 and SVF leads to superior bone formation and mineralization. The synergy between rhBMP-2's osteoinductive properties and SVF's angiogenic potential resulted in the most robust and well-integrated bone tissue among the experimental groups. These findings reaffirm that the in vitro benefits of rhBMP-2 and SVF can be effectively translated into improved spinal fusion outcomes in a living organism, suggesting promising implications for their use in clinical settings to enhance bone regeneration and repair.

3.5. Evaluation of spinal fusion efficacy and bone regeneration through kinetic testing and Micro-CT analysis in the minipig OLIF model

In this study, we evaluated the efficacy of rhBMP-2 and hSVF cell transplantation using a minipig OLIF (Oblique Lateral Interbody Fusion) model, which provides greater clinical relevance than the rat PLF model. While PLF is still used in cases where interbody fusion cannot be performed or when sufficient fusion can be expected, interbody fusion surgeries such as OLIF, anterior, posterior, and transforaminal lumbar interbody fusion are preferred for achieving robust fusion outcomes. The minipig model was chosen due to its anatomical similarities to the human spine, including vertebral body height and bone density, making it a reliable animal model for studying spinal fusion techniques [59,60].

The OLIF procedure was performed at lumbar vertebral levels 2–3 and 4–5, and the fusion mass was evaluated through kinematic testing and micro-CT analysis at 8 and 16 weeks post-surgery (Fig. 5A).

In the kinematic tests, which evaluated the mobility of the vertebrae around the fusion site, most groups displayed some degree of movement at 8 weeks, but minimal movement at 16 weeks. Notably, in the rhBMP-

2 + SVF group, almost no lateral or forward bending was observed even at 8 weeks, suggesting that fusion occurred more efficiently in this group compared to the others (Fig. 5B and C). In contrast, the ABG group still exhibited some degree of lateral bending at 16 weeks, indicating a slower and less efficient fusion process compared to the rhBMP-2 and rhBMP-2 + SVF groups. These findings suggest that the combined use of rhBMP-2 and SVF can significantly accelerate the fusion process compared to traditional autologous bone grafting.

Micro-CT analysis further corroborated these findings, showing that the rhBMP-2 + SVF group had the most robust bone regeneration, with minimal soft tissue presence inside the fusion cage. The ABG and rhBMP-2 groups showed more soft tissue and less bone tissue at both 8 and 16 weeks, indicating incomplete fusion. In contrast, the rhBMP-2 + SVF group exhibited complete fusion, with the vertebral body and implanted BGM fusing effectively, leaving only trace amounts of the remaining carrier material (Fig. 5D). This suggests that the SVF and rhBMP-2 combination not only promotes rapid osteogenesis but also enhances the integration of the graft material, resulting in higher quality bone fusion. To analyze the regenerated bone in more detail, we focused on newly generated cancellous bone. Detailed analysis of the newly generated cancellous bone revealed a higher bone volume fraction in the rhBMP-2 and rhBMP-2 + SVF groups compared to the ABG group at both 8 and 16 weeks. The increase in trabecular number, along with a reduction in trabecular separation, contributed to the higher bone volume in these groups. Interestingly, the cancellous bone thickness in the rhBMP-2 + SVF group, which was initially lower at 8 weeks, increased to values comparable to those observed at 16 weeks, indicating continued bone maturation over time (Fig. 5E). These results demonstrate that the combination of rhBMP-2 and SVF significantly improves both the quantity and quality of newly fused bone, leading to more stable and durable spinal fusion.

The kinetic testing and micro-CT analysis further supported the superior outcomes of rhBMP-2 and SVF observed in the previous in vitro and rat PLF models. The combination of rhBMP-2 and SVF significantly improved both spinal fusion efficiency and bone regeneration in the minipig OLIF model, showing more robust and consistent bone formation compared to the autologous bone graft group. This synergistic effect between rhBMP-2's osteoinductive properties and SVF's vascularization potential was reflected in enhanced bone integration and minimized soft tissue interference, surpassing the efficacy of traditional autografting techniques. These findings suggest that the combination therapy can be clinically translated into a more effective spinal fusion strategy, offering significant advantages over conventional methods, such as reduced variability and faster recovery times.

3.6. Evaluation of bone formation and mineralization through histological analysis in the minipig OLIF model

Histological analysis was performed on the harvested spinal tissue samples to assess bone formation, mineralization, and the integration of the graft materials at 8 and 16 weeks post-surgery. Three staining methods—HE, GT, and VK—were used, consistent with the protocols applied in the rat model experiments.

Histological evaluation was conducted using hematoxylin and eosin (HE) staining to assess the overall tissue morphology and the extent of new bone formation within the defective site in the OLIF-performed tissues. The rectangular area of the defect inside the cage was
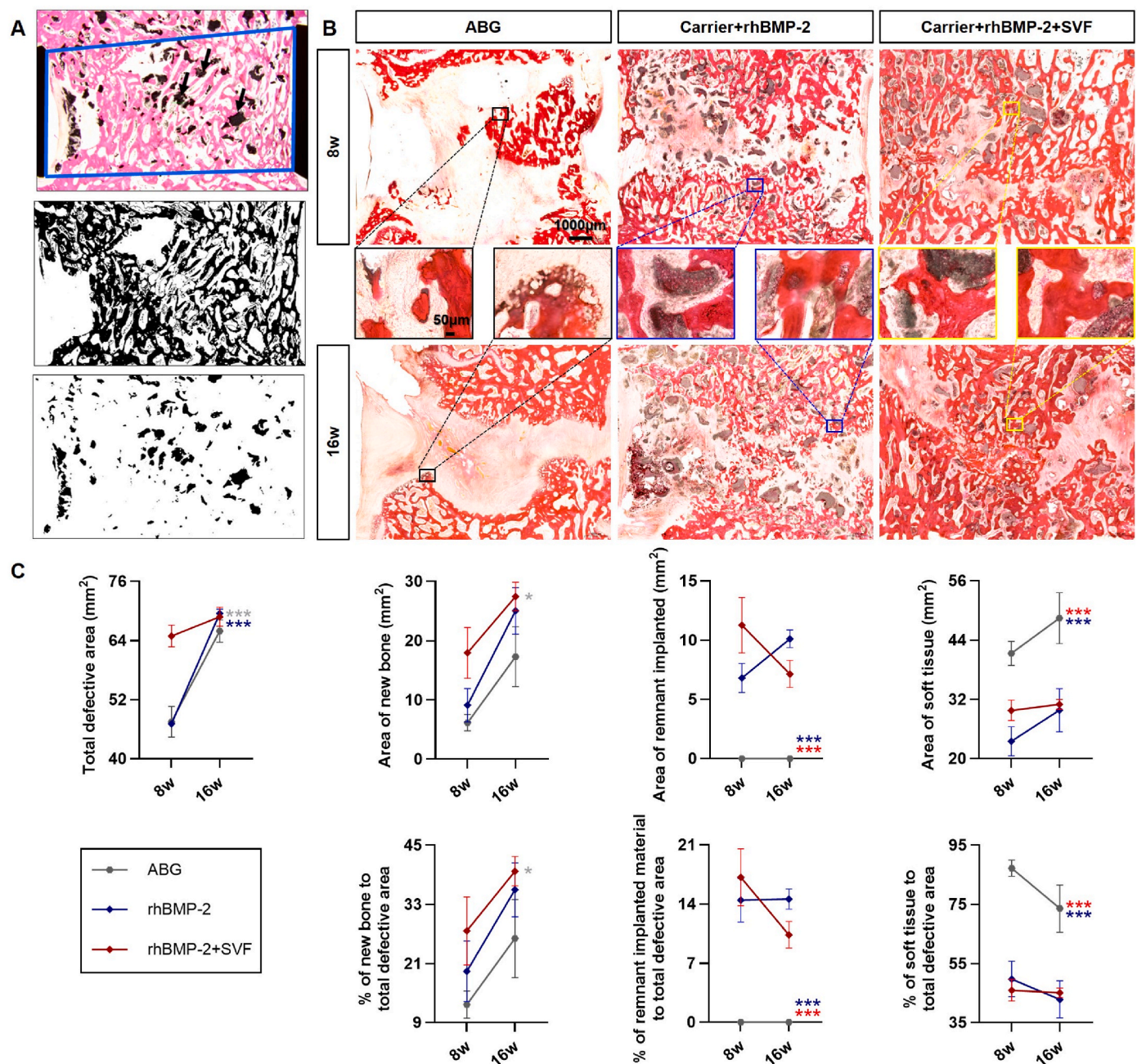
Fig. 6. Histological analysis the fusion mass at 8 and 16 weeks after OLIF in the minipig model.
A) Measurement of the area of newly formed bone and residual implant in the defective area. The square area in the first picture is located inside the cage as the area selected for measurement. The second and third pictures respectively indicate the area of newly formed bone tissue and the remaining implanted materials in the selected defective area. B) Histological HE staining of the fusion site including the end plate of the vertebral body centering on the cage implantation site containing ABG. C) Comparison of the areas of newly formed bone, the remaining implanted materials, and soft tissue in the selected defective area of each group on 8 weeks and 16 weeks after the implantation. $*p < 0.05$, $**p < 0.01$, and $***p < 0.001$ indicate statistically significant differences.

measured, averaging 47–65 mm², with new bone formation predominantly occurring in the form of trabecular bone (Fig. 6A). Among the groups, the rhBMP-2 + SVF group exhibited the highest level of new bone formation at the defect site after both 8 weeks (17.97 ± 4.274 mm²) and 16 weeks (27.45 ± 2.412 mm²), surpassing the rhBMP-2 group (9.124 ± 2.815 mm² at 8 weeks and 25.07 ± 3.905 mm² at 16 weeks) and the ABG group (6.178 ± 1.381 mm² at 8 weeks and 17.31 ± 5.063 mm² at 16 weeks). An inverse relationship was observed between the proportion of soft tissue and the area occupied by newly formed bone. The ABG group demonstrated the highest proportion of soft tissue at both 8 weeks (41.35 ± 2.443 mm²) and 16 weeks (48.49 ± 5.136

mm²), while the rhBMP-2 + SVF group exhibited significantly reduced soft tissue presence (29.79 ± 2.077 mm² at 8 weeks and 31.01 ± 0.982 mm² at 16 weeks). The rhBMP-2 group showed intermediate values (23.55 ± 2.941 mm² at 8 weeks and 29.84 ± 4.370 mm² at 16 weeks). Importantly, in the rhBMP-2 + SVF group, the newly formed bone fused effectively with both the upper and lower vertebral bodies, indicating more complete and efficient bone fusion compared to autologous bone grafting (ABG). Additionally, small amounts of residual implanted materials were observed in the SVF and rhBMP-2 + SVF groups at both 8 and 16 weeks, suggesting that the HA and TH components of the bone graft material (BGM) were largely utilized in the bone fusion process.

This efficient utilization of the graft material further supports the enhanced bone regeneration observed in the rhBMP-2 + SVF group (Fig. 6B and C).

GT staining confirmed the synthesis of both organic and inorganic bone, with the rhBMP-2 + SVF group showing the highest level of mineralization (blue-green) compared to the other groups (Fig. 7A–C). In the ABG group, fibrous tissue dominated the defect site, and the presence of ceramic carriers in the rhBMP-2 group suggested incomplete bone mineralization. However, in the rhBMP-2 + SVF group, the majority of the osteoid region was mineralized, resulting in the most well-developed bone structure.

VK staining was used to identify Ca^{2+}-positive regions, providing further insights into the degree of mineralization. At 8 weeks, the rhBMP-2 + SVF group exhibited the largest Ca^{2+}-positive regions, indicating that the combination of rhBMP-2 and SVF accelerated the mineralization process. Interestingly, by 16 weeks, there was no significant difference in the Ca^{2+}-positive areas between the rhBMP-2 and rhBMP-2 + SVF groups, suggesting that mineralization plateaued after 8 weeks in the rhBMP-2 + SVF group, while the rhBMP-2 group continued to mineralize over time (Fig. 7D–F). This rapid mineralization in the rhBMP-2 + SVF group may contribute to faster stabilization of the fusion site and reduce the risk of heterotopic ossification.

The histological analysis of the minipig OLIF model confirmed that the combination of hSVF cells and low-dose rhBMP-2 resulted in the
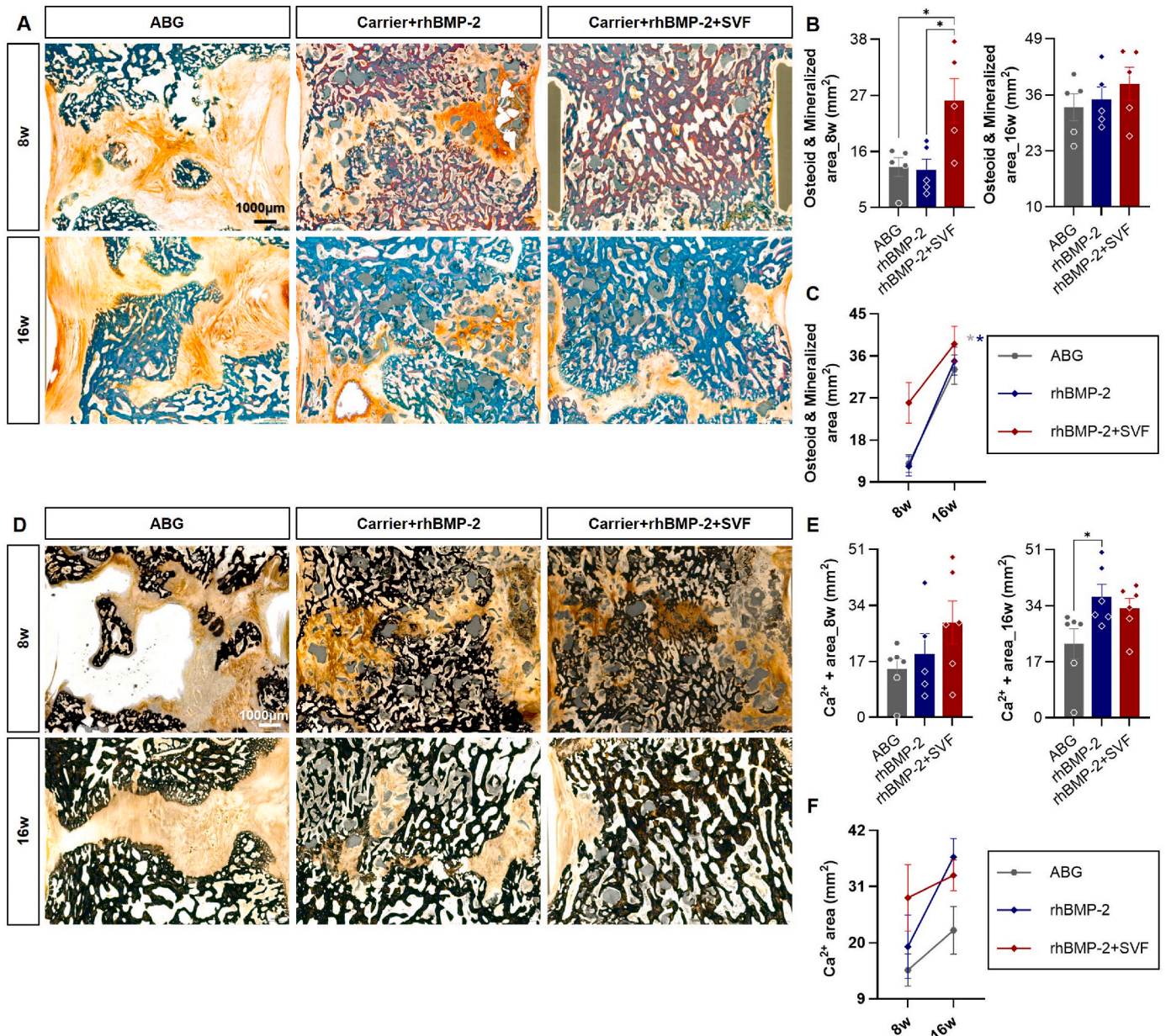

Fig. 7. Mineralization analysis of fusion mass at 8 and 16 weeks after OLIF in the minipig model.
A) Histological GT staining of the fusion site including the end plate of the vertebral body centering on the cage implantation site containing ABG. B) Analysis of the osteoid and mineralized areas at 8 weeks and 16 weeks. C) Changes in osteoid and mineralized area with respect to group and week. D) Histological VK staining of the fusion site including the end plate of the vertebral body centering on the cage implantation site containing ABG. E) Analysis of the Ca^{2+}-positive area at 8 weeks and 16 weeks. F) Changes in Ca^{2+} area with respect to group and week. rhBMP-2 increased in the groups with ceramic carriers (purple) and degenerated organic tissue into inorganic tissue at 16 weeks, greatly increasing mineralized areas. During this mineralization, Ca^{2+}-positive regions increased more rapidly when hSVF cells were implanted together with rhBMP-2 rather than when rhBMP-2 was implanted alone, and the area did not increase significantly and remained stable at 16 weeks. *$p < 0.05$, **$p < 0.01$, and ***$p < 0.001$ indicate statistically significant differences.

fastest and most complete bone formation, with minimal soft tissue interference. This synergistic effect significantly enhanced both the quantity and quality of newly formed bone compared to the autologous bone graft group. The combined use of rhBMP-2 and SVF not only accelerated bone maturation but also improved mineralization and integration, stabilizing the fusion mass more effectively than either treatment alone. These findings demonstrate that the synergistic effects observed in vitro and in the rat PLF model translate successfully to a more clinically relevant minipig model, highlighting the potential for this combination therapy to offer a more reliable and efficient alternative to autologous bone grafts in spinal fusion surgery.

4. Discussion

The efficacy of rhBMP-2 in spinal fusion is well-established, primarily due to its strong osteoinductive properties. Previous studies have demonstrated that patients receiving high doses of rhBMP-2, typically between 8.4 and 12 mg (as seen with INFUSE), exhibited significantly higher fusion rates (98 % compared to 76 % for iliac crest bone graft), with additional benefits such as reduced surgery duration, blood loss, and shorter hospital stays [61]. However, the use of such high-dose rhBMP-2, particularly in anterior lumbar interbody fusion, has also been associated with a range of complications, including inflammation, radiculopathy, heterotopic ossification, osteolysis, subsidence, and even potential tumor facilitation [12,62,63]. The FDA's (Food and Drug Administration) rejection of the high-dose rhBMP-2 product AMPLIFY in 2011, due to concerns over increased cancer risk, highlighted the critical need for safer, lower-dose delivery methods for rhBMP-2 [11]. To address these concerns, we proposed the use of a novel bio ceramic carrier with sustained-release and localized retention properties for rhBMP-2, capable of maintaining its osteoinductive effects while reducing the risk of complications associated with high doses. Unlike the commonly used high doses of rhBMP-2 (8.4–12 mg) in previous studies, our research employed a significantly reduced dose of 0.4 mg/cc. This lower dose was specifically designed to minimize the adverse effects linked to high-dose rhBMP-2 while still ensuring effective bone regeneration.

In our previous studies, we confirmed that a mechanical mixture of HA and TH could deliver rhBMP-2 effectively [32]. HA and β-TCP have excellent reabsorbability, biocompatibility, and bone conductivity, making them ideal carriers for bone regeneration [64–66]. These materials promote bone remodeling and osseointegration by providing essential minerals like Ca^{2+} and PO_4^{3-}, supporting the bone regeneration process [67,68]. By adjusting the HA-to-TH ratio, we achieved a controlled degradation rate, allowing for sustained release of rhBMP-2 and enhanced bone formation.

To further improve the sustained release of rhBMP-2, we modified the ratio of HA and β-TCP + hydrogel from 1:2 to 2:3. This adjustment effectively prevented the initial over-release of rhBMP-2 and extended its release duration up to 3 weeks, providing a more controlled and gradual delivery of rhBMP-2. This improvement ensures a more consistent supply of rhBMP-2 during the critical early stages of bone healing, enhancing the osteoinductive effect and reducing the risk of rapid clearance (Fig. 1A–C). Moreover, by preventing the initial over-release, this system allowed us to achieve the desired bone healing effects with a much lower dose of rhBMP-2. As a result, we were able to use a significantly reduced amount of rhBMP-2 compared to conventional methods, minimizing potential side effects associated with higher doses while still maintaining effective bone regeneration. This optimized delivery system not only maximizes the efficiency of rhBMP-2 but also enhances the safety profile of the treatment.

Furthermore, the use of hydrogels in combination with β-TCP represents a promising strategy for controlled drug delivery. Hydrogels, with their highly porous and hydrophilic structure, provide an ideal environment for cellular infiltration and vascularization. Their ability to act as drug reservoirs, enabling controlled, on-demand release of

bioactive factors, makes them especially suited for bone tissue engineering applications [69,70]. In our study, we used a hydrogel mixture made of Poloxamer 407 and HPMC. Poloxamer 407 is a biodegradable, non-toxic polymer known for its temperature-dependent thermal conformation, while HPMC helps maintain the hydrogel structure [34, 37–39]. Together, these components in a 1:1 wt ratio promote the slow and sustained release of rhBMP-2, ensuring a controlled delivery within the BGM. This microsphere-type hydrogel combined with β-TCP not only prevented the initial over-release of rhBMP-2 but also ensured sustained release, promoting osteodifferentiation and improving the stability of the BGM at the implant site.

Additionally, a study reported by Japanese researchers demonstrated that the novel bioceramic formulation (HAp/β-TCP hydrogel, Novosis Putty) exhibited superior sustained release and localized retention of rhBMP-2 compared to traditional collagen sponge carriers [34–36]. In vitro release studies, 98.3 % of rhBMP-2 loaded onto collagen sponge was released within 1–7 days, while the HAp/β-TCP hydrogel demonstrated sustained release for up to 24 days. In vivo, rhBMP-2 delivered via the hydrogel exhibited a longer biological half-life, enhanced osteogenic gene expression, and superior bone formation in a rat spinal fusion model. In a rat intervertebral fusion model, the fusion rate in the HAp/β-TCP hydrogel group (87.5 %) was significantly higher than in the collagen sponge group (low dose: 50 %, high dose: 62.5 %). Bone formation with the hydrogel was confined to the disc space, whereas ectopic bone was observed with collagen sponge. Furthermore, the hydrogel group showed abundant thick trabecular bone, in contrast to the collagen sponge group, which predominantly resulted in fatty bone marrow. From a safety perspective, the hydrogel group exhibited no dose-dependent soft tissue swelling, while the collagen sponge group showed significantly increased swelling at high doses.

Another critical aspect of spinal fusion is the role of MSCs, which can differentiate into osteoblasts and significantly contribute to bone formation. During spinal fusion surgery, when cortical bone is removed by decortication, the MSCs within the exposed trabecular bone can be utilized. MSCs are undifferentiated cells known for their high growth rates and potential to differentiate into osteoblasts, making them a promising candidate for bone tissue engineering [71,72]. However, their clinical application is limited by their scarcity in bone tissue, the complexity of culturing techniques, and the need for sterile environments, all of which contribute to high costs and lengthy preparation times [73–75].

In contrast, SVF cells offer a more accessible and practical alternative. SVF, derived from adipose tissue, contains a diverse population of cells, including MSCs, pericytes, endothelial progenitor cells, and immune cells. These cell types collectively enhance angiogenesis, promote tissue repair, and modulate immune responses, making SVF a valuable resource for spinal fusion and other regenerative therapies [50,76]. Due to its accessibility and rich cellular composition, SVF is emerging as a more viable option for clinical applications compared to traditional MSC-based therapies [27]. In orthopedic surgery, SVF cells have further been utilized to treat arthritis, fractures, and lumbar spine fusion in orthopedic surgery, and clinical implications have been widely researched [76–79].

Angiogenesis is a critical factor for successful spinal fusion, as it supports the development of a functional vascular network necessary for bone healing. Tissue engineering strategies require scaffolds that not only promote bone formation but also guide immune responses, enable controlled degradation, and, importantly, facilitate angiogenesis to ensure long-term fusion success [80]. Although prior research has highlighted the potential of SVF in promoting either bone formation or angiogenesis individually, clear evidence demonstrating its capacity to simultaneously enhance both processes has been lacking. In our study, we provided new evidence that SVF cells possess the dual ability to promote both osteogenesis and angiogenesis. Angiogenesis was confirmed in in vitro cell culture experiments, where SVF significantly upregulated the gene expression of VEGF-A and Angiopoietin-1—key

regulators of angiogenesis—and increased CD31 expression, a marker of vascular endothelial cells (Fig. 2). This demonstrated SVF's strong angiogenic potential. In addition to the in vitro findings, the osteogenic effects of SVF were validated in in vivo models. In the rat PLF model, the combination of rhBMP-2 and SVF significantly enhanced bone fusion and improved bone quality. Furthermore, in the minipig OLIF model, which closely resembles clinical conditions, SVF, when combined with rhBMP-2, facilitated superior bone formation and integration, providing robust evidence of SVF's osteogenic capabilities in a more clinically relevant context (Figs. 1, 3–7).

Interestingly, no inflammatory response was observed in our histological analysis, likely due to the high proportion of M2 macrophages in the SVF, which are known for their anti-inflammatory and tissue-repairing functions. M2 macrophages release cytokines such as interleukin-10 (IL-10) and growth factors like TGF-β and VEGF, which contribute to wound healing and angiogenesis [81,82]. This anti-inflammatory effect further enhances the therapeutic potential of SVF in spinal fusion.

While our study demonstrates the efficacy of low-dose rhBMP-2 in combination with SVF for spinal fusion, several areas warrant further investigation. Although the sustained release system using a novel carrier significantly improved bone formation and osteointegration in both in vitro and in vivo models, there are still limitations when translating these results to clinical settings. Differences in biological structures and responses between animals and humans may influence the long-term safety and efficacy of this approach.

Furthermore, the synergistic effect observed between rhBMP-2 and SVF in our study was more pronounced in in vitro models compared to in vivo experiments, particularly in minipig models. This reduced effect in vivo may be attributed to the relatively small number of SVF cells transplanted per level, as SVF isolated from a single donor's adipose tissue was divided and distributed across four spinal levels in minipigs. Future studies should address this limitation by focusing on transplanting SVF into 1–2 levels per donor to better evaluate its potential synergistic effects with rhBMP-2. Thus, future studies should focus on long-term assessments to evaluate potential risks, such as ectopic bone formation, immune responses, or adverse inflammatory reactions. Additionally, direct comparisons with conventional treatments like autologous bone grafting are essential to fully understand the advantages and limitations of this novel therapeutic strategy. Human clinical trials will be critical to confirm these findings and optimize the application of this therapy for broader orthopedic use. Despite these limitations, our findings provide a robust foundation for sustained rhBMP-2 release and suggest that the combination of osteoinductive materials and SVF could represent a highly effective scaffold for spinal fusion and other bone regeneration therapies.

5. Conclusion

Our study presents a novel approach to spinal fusion by combining low-dose recombinant human bone morphogenetic protein-2 (rhBMP-2) with stromal vascular fraction (SVF) in an injectable hydrogel composite. This formulation leverages the biphasic ceramic structure of hydroxyapatite (HA)/beta-tricalcium phosphate (β-TCP) and a hydrogel matrix, enabling the controlled release of rhBMP-2 and promoting osteogenesis and angiogenesis. Importantly, the reduced rhBMP-2 dose addresses safety concerns while maintaining efficacy.

Preclinical studies using rat posterolateral fusion (PLF) and minipig oblique lateral interbody fusion (OLIF) models demonstrated significant improvements in bone density, vascularization, and graft integration. These findings underscore the synergistic effects of rhBMP-2 and SVF, critical for successful spinal fusion.

While further studies are needed to confirm clinical applicability, this composite material offers a promising strategy for safer, more effective bone regeneration therapies, laying the foundation for advancements in regenerative medicine and biomaterials research.

CRediT authorship contribution statement

Hye Yeong Lee: Writing – review & editing, Writing – original draft, Visualization, Validation, Project administration, Methodology, Investigation, Formal analysis, Data curation, Conceptualization. **Seong Bae An:** Writing – review & editing, Writing – original draft, Methodology, Investigation, Funding acquisition, Conceptualization. **Sae Yeon Hwang:** Visualization, Validation, Investigation. **Gwang Yong Hwang:** Visualization, Validation, Investigation. **Hye-Lan Lee:** Writing – original draft, Methodology, Investigation. **Hyun Jung Park:** Writing – review & editing, Resources, Methodology, Investigation, Funding acquisition. **Joongkyum Shin:** Writing – review & editing, Writing – original draft. **Keung Nyun Kim:** Supervision, Project administration, Conceptualization. **Sung Won Wee:** Validation, Investigation. **Sol Lip Yoon:** Investigation. **Yoon Ha:** Supervision, Project administration, Methodology, Funding acquisition, Conceptualization.

Ethics approval statements

All rat care and surgeries were performed in accordance with Association for Assessment and Accreditation of Laboratory Animal Care (AAALAC) regulations and were managed and supervised with Institutional Animal Care and Use Committee at Yonsei university college of medicine (IACUC; protocol number: 2020-0326) approval.

Mini-pig surgery and breeding were managed and supervised according to a protocol approved by the IACUC at Yonsei university college of medicine (protocol number: 2019-0061) in accordance with AAALAC regulations, similar to the small animal experiments.

All hSVF obtained according to established protocols, with the consent of all patients, and in accordance with established standards of the Severance Hospital Institutional Review Board (approval number: 4-2020-1121).

Availability of data and materials

The drugs used in the study can be purchased at Sigma-Aldrich now. In addition, the data that support the findings of this study are available from the corresponding authors upon request.

Declaration of competing interest

The authors declare the following financial interests/personal relationships which may be considered as potential competing interests: Hyun Jung Park has patent #INJECTABLE CALCIUM PHOSPHATE-BASED BONE GRAFT COMPOSITE HAVING HIGH ELASTICITY AND PREPARATION METHOD THEREOF licensed to 10-2020-0127278 (PCT: WO 2022/071636 A1) licensed to licensed. If there are other authors, they declare that they have no known competing financial interests or personal relationships that could have appeared to influence the work reported in this paper.

Acknowledgements

List of abbreviations

AAALAC   Assessment and Accreditation of Laboratory Animal Care
ABG   Autologous Bone Graft

ADSCs	Adipose-Derived Stem Cells
ALP	Alkaline Phosphatase
Ang1	Angiopoietin-1
BCP	Biphasic Calcium Phosphate
BGM	Bone Graft Material
BMPs	Bone Morphogenetic Proteins
DMEM	Dulbecco's Modified Eagle Medium
ECs	Endothelial Cells
ELISA	Enzyme-Linked Immunosorbent Assay
FBs	Fibroblasts
FBS	Fetal Bovine Serum
GT	Goldner's Trichrome
HA	Hydroxyapatite
HE	Hematoxylin and Eosin
hMSCs	Human Mesenchymal Stem Cells
hSVF	Human Adipose Tissue Derived Stromal Vascular Fraction
HPMC	Hydroxypropyl Methylcellulose
IACUC	Institutional Animal Care and Use Committee
ICBG	Iliac Crest Bone Graft
micro-CT	Micro-Computed Tomography
MSCs	Mesenchymal Stem Cells
OCN	Osteocalcin
OLIF	Oblique Lateral Interbody Fusion
PBS	Phosphate-Buffered Saline
PEEK	Polyetheretherketone
PLF	Posterolateral Fusion
rSVF	Rat Adipose Tissue-Derived Stromal Vascular Fraction
rhBMP-2	Recombinant Human Bone Morphogenetic Proteins −2
RUNX2	Runt-Related Transcription Factor 2
SVF	Stromal Vascular Fraction
TCP	Tricalcium Phosphate
TGF-β	Transforming Growth Factor-Beta
VK	Von Kossa

Data availability

Data will be made available on request.

References

[1] T.S. Montenegro, C. Elia, K. Hines, Z. Buser, J. Wilson, Z. Ghogawala, S.N. Kurpad, D.M. Sciubba, J.S. Harrop, Are lumbar fusion guidelines followed? A survey of north American spine surgeons, Neurospine 18 (2) (2021) 389–396, https://doi.org/10.14245/ns.2142136.068.

[2] B.I. Martin, S.K. Mirza, N. Spina, W.R. Spiker, B. Lawrence, D.S. Brodke, Trends in lumbar fusion procedure rates and associated hospital costs for degenerative spinal diseases in the United States, 2004 to 2015, Spine (Phila Pa 44 (5) (1976) 369–376, https://doi.org/10.1097/BRS.0000000000002822.

[3] M.C. Prabhu, K.C. Jacob, M.R. Patel, H. Pawlowski, N.N. Vanjani, K. Singh, History and evolution of the minimally invasive transforaminal lumbar interbody fusion, Neurospine 19 (3) (2022) 479–491, https://doi.org/10.14245/ns.2244122.061.

[4] A.M. Jakoi, J.A. Iorio, P.J. Cahill, Autologous bone graft harvesting: a review of grafts and surgical techniques, Musculoskelet. Surg. 99 (3) (2015) 171–178, https://doi.org/10.1007/s12306-015-0351-6.

[5] C.E. Gillman, A.C. Jayasuriya, FDA-approved bone grafts and bone graft substitute devices in bone regeneration, Mater. Sci. Eng. C Mater. Biol. Appl. 130 (2021) 112466, https://doi.org/10.1016/j.msec.2021.112466.

[6] J. Kim, S. Lee, Y. Choi, J. Choi, B.J. Kang, Sustained release of bone morphogenetic protein-2 through alginate microbeads enhances bone regeneration in rabbit tibial metaphyseal defect model, Materials 14 (10) (2021), https://doi.org/10.3390/ma14102600.

[7] Z. Wu, B. Zhou, L. Chen, X. Wang, M.E.A. Abdelrahim, C. Wei, Bone morphogenetic protein-2 against iliac crest bone graft for the posterolateral fusion of the lumbar spine: a meta-analysis, Int. J. Clin. Pract. 75 (4) (2021) e13911, https://doi.org/10.1111/ijcp.13911.

[8] H.Y. Choi, S.J. Hyun, C.H. Lee, J.H. Youn, M.Y. Ryu, K.J. Kim, Safety and efficacy of recombinant human bone morphogenetic protein-2 in multilevel posterolateral lumbar fusion in a prospective, randomized, controlled trial, Neurospine 19 (3) (2022) 838–846, https://doi.org/10.14245/ns.2244464.232.

[9] R. Agarwal, K. Williams, C.A. Umscheid, W.C. Welch, Osteoinductive bone graft substitutes for lumbar fusion: a systematic review, J. Neurosurg. Spine 11 (6) (2009) 729–740, https://doi.org/10.3171/2009.6.SPINE08669.

[10] C.J. Hwang, J.H. Lee, H.R. Baek, B.S. Chang, C.K. Lee, Evaluation of the efficacy of Escherichia coli-derived recombinant human bone morphogenetic protein-2 in a mini-pig spinal anterior interbody fusion model, Bone Joint Lett. J 95-B (2) (2013) 217–223, https://doi.org/10.1302/0301-620X.95B2.29466.

[11] A. Mesfin, J.M. Buchowski, L.P. Zebala, W.R. Bakhsh, A.B. Aronson, J.L. Fogelson, S. Hershman, H.J. Kim, A. Ahmad, K.H. Bridwell, High-dose rhBMP-2 for adults: major and minor complications: a study of 502 spine cases, J. Bone Joint Surg. Am. 95 (17) (2013) 1546–1553, https://doi.org/10.2106/JBJS.L.01730.

[12] A.W. James, G. LaChaud, J. Shen, G. Asatrian, V. Nguyen, X. Zhang, K. Ting, C. Soo, A review of the clinical side effects of bone morphogenetic protein-2, Tissue Eng. Part B Rev. 22 (4) (2016) 284–297, https://doi.org/10.1089/ten.TEB.2015.0357.

[13] V. Tollemar, Z.J. Collier, M.K. Mohammed, M.J. Lee, G.A. Ameer, R.R. Reid, Stem cells, growth factors and scaffolds in craniofacial regenerative medicine, Genes Dis 3 (1) (2016) 56–71, https://doi.org/10.1016/j.gendis.2015.09.004.

[14] J.W. Arner, R.D. Santrock, A historical review of common bone graft materials in foot and ankle surgery, Foot Ankle Spec. 7 (2) (2014) 143–151, https://doi.org/10.1177/1938640013516358.

[15] S. Bansal, V. Chauhan, S. Sharma, R. Maheshwari, A. Juyal, S. Raghuvanshi, Evaluation of hydroxyapatite and beta-tricalcium phosphate mixed with bone marrow aspirate as a bone graft substitute for posterolateral spinal fusion, Indian J. Orthop. 43 (3) (2009) 234–239, https://doi.org/10.4103/0019-5413.49387.

[16] J. Jeong, J.H. Kim, J.H. Shim, N.S. Hwang, C.Y. Heo, Bioactive calcium phosphate materials and applications in bone regeneration, Biomater. Res. 23 (2019) 4, https://doi.org/10.1186/s40824-018-0149-3.

[17] J.M. Bouler, P. Pilet, O. Gauthier, E. Verron, Biphasic calcium phosphate ceramics for bone reconstruction: a review of biological response, Acta Biomater. 53 (2017) 1–12, https://doi.org/10.1016/j.actbio.2017.01.076.

[18] V. Arisan, T. Ozdemir, A. Anil, J.A. Jansen, K. Ozer, Injectable calcium phosphate cement as a bone-graft material around peri-implant dehiscence defects: a dog study, Int. J. Oral Maxillofac. Implants 23 (6) (2008) 1053–1062.

[19] A.S. Akay, V. Arisan, E. Cevher, M. Sessevmez, B. Cam, Oxytocin-loaded sustained-release hydrogel graft provides accelerated bone formation: an experimental rat study, J. Orthop. Res. 38 (8) (2020) 1676–1687, https://doi.org/10.1002/jor.24607.

[20] M.S. Akash, K. Rehman, Recent progress in biomedical applications of Pluronic (PF127): pharmaceutical perspectives, J. Control. Release 209 (2015) 120–138, https://doi.org/10.1016/j.jconrel.2015.04.032.

[21] A. Torcello-Gomez, M. Wulff-Perez, M.J. Galvez-Ruiz, A. Martin-Rodriguez, M. Cabrerizo-Vilchez, J. Maldonado-Valderrama, Block copolymers at interfaces: interactions with physiological media, Adv. Colloid Interface Sci. 206 (2014) 414–427, https://doi.org/10.1016/j.cis.2013.10.027.

[22] E. Giuliano, D. Paolino, M. Fresta, D. Cosco, Mucosal applications of poloxamer 407-based hydrogels: an overview, Pharmaceutics 10 (3) (2018).

[23] P. Pan, D. Svirskis, G.I.N. Waterhouse, Z.M. Wu, Hydroxypropyl methylcellulose bioadhesive hydrogels for topical application and sustained drug release: the effect of polyvinylpyrrolidone on the physicomechanical properties of hydrogel, Pharmaceutics 15 (9) (2023).

[24] D.E. Ciolacu, R. Nicu, F. Ciolacu, Cellulose-based hydrogels as sustained drug-delivery systems, Materials 13 (22) (2020).

[25] E. Russo, C. Villa, Poloxamer hydrogels for biomedical applications, Pharmaceutics 11 (12) (2019), https://doi.org/10.3390/pharmaceutics11120671.

[26] P. Bora, A.S. Majumdar, Adipose tissue-derived stromal vascular fraction in regenerative medicine: a brief review on biology and translation, Stem Cell Res. Ther. 8 (1) (2017) 145, https://doi.org/10.1186/s13287-017-0598-y.

[27] I. Andia, N. Maffulli, N. Burgos-Alonso, Stromal vascular fraction technologies and clinical applications, Expert Opin. Biol. Ther 19 (12) (2019) 1289–1305, https://doi.org/10.1080/14712598.2019.1671970.

[28] L. Charles-de-Sa, N.F. Gontijo-de-Amorim, C. Maeda Takiya, R. Borojevic, D. Benati, P. Bernardi, A. Sbarbati, G. Rigotti, Antiaging treatment of the facial skin by fat graft and adipose-derived stem cells, Plast. Reconstr. Surg. 135 (4) (2015) 999–1009, https://doi.org/10.1097/PRS.0000000000001123.

[29] E.P. Tracy, R. Nair, G. Rowe, J.E. Beare, A. Beyer, A.J. LeBlanc, Adipose stromal vascular fraction reverses mitochondrial dysfunction and hyperfission in aging-induced coronary microvascular disease, Am. J. Physiol. Heart Circ. Physiol. 323 (4) (2022) H749–H762, https://doi.org/10.1152/ajpheart.00311.2022.

[30] A. Stachura, W. Paskal, W. Pawlik, M.J. Mazurek, J. Jaworowski, The use of adipose-derived stem cells (ADSCs) and stromal vascular fraction (SVF) in skin scar treatment-A systematic review of clinical studies, J. Clin. Med. 10 (16) (2021), https://doi.org/10.3390/jcm10163637.

[31] K. Wittmann, N. Dietl, N. Ludwig, O. Berberich, C. Hoefner, K. Storck, T. Blunk, P. Bauer-Kreisel, Engineering vascularized adipose tissue using the stromal-vascular fraction and fibrin hydrogels, Tissue Eng. Part A 21 (7–8) (2015) 1343–1353, https://doi.org/10.1089/ten.TEA.2014.0299.

[32] H.Y. Lee, J.I. Kang, H.L. Lee, G.Y. Hwang, K.N. Kim, Y. Ha, Concentration-dependent efficacy of recombinant human bone morphogenetic protein-2 using a HA/beta-TCP hydrogel carrier in a mini-pig vertebral oblique lateral interbody fusion model, Int. J. Mol. Sci. 24 (1) (2023), https://doi.org/10.3390/ijms24010892.

[33] D. Tateiwa, S. Nakagawa, H. Tsukazaki, R. Okada, J. Kodama, J. Kushioka, Z. Bal, Y. Ukon, H. Hirai, T. Kaito, A novel BMP-2-loaded hydroxyapatite/beta-tricalcium phosphate microsphere/hydrogel composite for bone regeneration, Sci. Rep. 11 (1) (2021), https://doi.org/10.1038/s41598-021-96484-4.

[34] D. Tateiwa, S. Nakagawa, H. Tsukazaki, R. Okada, J. Kodama, J. Kushioka, Z. Bal, Y. Ukon, H. Hirai, T. Kaito, A novel BMP-2-loaded hydroxyapatite/beta-tricalcium phosphate microsphere/hydrogel composite for bone regeneration, Sci. Rep. 11 (1) (2021) 16924, https://doi.org/10.1038/s41598-021-96484-4.

[35] S. Nakagawa, R. Okada, J. Kushioka, J. Kodama, H. Tsukazaki, Z. Bal, D. Tateiwa, Y. Ukon, H. Hirai, T. Makino, S. Takenaka, S. Okada, T. Kaito, Effects of rhBMP-2-loaded hydroxyapatite granules/beta-tricalcium phosphate hydrogel (HA/beta-TCP/hydrogel) composite on a rat model of caudal intervertebral fusion, Sci. Rep. 12 (1) (2022) 7906, https://doi.org/10.1038/s41598-022-12082-y.

[36] T. Kitahara, D. Tateiwa, H. Hirai, M. Ikuta, T. Furuichi, M. Bun, Y. Ukon, Y. Kanie, M. Furuya, T. Fujimori, S. Okada, T. Kaito, rhBMP-2-loaded hydroxyapatite/beta-tricalcium phosphate microsphere/hydrogel composite promotes bone regeneration in a novel rat femoral nonunion model, Front. Bioeng. Biotechnol. 12 (2024) 1461260, https://doi.org/10.3389/fbioe.2024.1461260.

[37] G. Dumortier, J.L. Grossiord, F. Agnely, J.C. Chaumeil, A review of poloxamer 407 pharmaceutical and pharmacological characteristics, Pharm. Res. (N. Y.) 23 (12) (2006) 2709–2728, https://doi.org/10.1007/s11095-006-9104-4.

[38] E. Giuliano, D. Paolino, M. Fresta, D. Cosco, Drug-loaded biocompatible nanocarriers embedded in poloxamer 407 hydrogels as therapeutic formulations, Medicines (Basel) 6 (1) (2018), https://doi.org/10.3390/medicines6010007.

[39] J.B. da Silva, M.T. Cook, M.L. Bruschi, Thermoresponsive systems composed of poloxamer 407 and HPMC or NaCMC: mechanical, rheological and sol-gel transition analysis, Carbohydr. Polym. 240 (2020) 116268, https://doi.org/10.1016/j.carbpol.2020.116268.

[40] H.J. Son, S.H. Choi, M.K. Lee, C.N. Kang, Efficacy and safety of Escherichia coli-derived recombinant human bone morphogenetic protein-2 in additional lumbar posterolateral fusion: minimum 1-year follow-up, Spine J. 21 (8) (2021) 1340–1346, https://doi.org/10.1016/j.spinee.2021.04.007.

[41] S.H. Choi, J.W. Koo, D. Choe, J.M. Hur, D.H. Kim, C.N. Kang, Interbody fusion in degenerative lumbar spinal stenosis with additional posterolateral fusion using Escherichia coli-derived bone morphogenetic protein-2: a Pilot study, Medicine (Baltim.) 99 (24) (2020) e20477, https://doi.org/10.1097/MD.0000000000020477.

[42] J.H. Cho, J.H. Lee, J.S. Yeom, B.S. Chang, J.J. Yang, K.H. Koo, C.J. Hwang, K.B. Lee, H.J. Kim, C.K. Lee, H. Kim, K.S. Suk, W.D. Nam, J. Han, Efficacy of Escherichia coli-derived recombinant human bone morphogenetic protein-2 in posterolateral lumbar fusion: an open, active-controlled, randomized, multicenter trial, Spine J. 17 (12) (2017) 1866–1874, https://doi.org/10.1016/j.spinee.2017.06.023.

[43] J.A. Aronowitz, R.A. Lockhart, C.S. Hakakian, A method for isolation of stromal vascular fraction cells in a clinically relevant time frame, Methods Mol. Biol. 1773 (2018) 11–19, https://doi.org/10.1007/978-1-4939-7799-4_2.

[44] R. Hearnden, B. Sandhar, V. Vyas, M.P. Longhi, Isolation of stromal vascular fraction cell suspensions from mouse and human adipose tissues for downstream applications, STAR Protoc. 2 (2) (2021) 100422, https://doi.org/10.1016/j.xpro.2021.100422.

[45] P.G. Cho, G.Y. Ji, Y. Ha, H.Y. Lee, D.A. Shin, Effect of the type of electrical stimulation on spinal fusion in a rat posterolateral spinal fusion model, Spine J. 19 (6) (2019) 1106–1120, https://doi.org/10.1016/j.spinee.2018.12.011.

[46] H.Y. Lee, D.S. Kim, G.Y. Hwang, J.K. Lee, H.L. Lee, J.W. Jung, S.Y. Hwang, S.W. Baek, S.L. Yoon, Y. Ha, K.N. Kim, I. Han, D.K. Han, C.K. Lee, Multi-modulation of immune-inflammatory response using bioactive molecule-integrated PLGA composite for spinal fusion, Mater. Today Bio 19 (2023) 100611, https://doi.org/10.1016/j.mtbio.2023.100611.

[47] D.A. Shin, B.M. Yang, G. Tae, Y.H. Kim, H.S. Kim, H.I. Kim, Enhanced spinal fusion using a biodegradable porous mesh container in a rat posterolateral spinal fusion model, Spine J. 14 (3) (2014) 408–415, https://doi.org/10.1016/j.spinee.2013.08.038.

[48] D. Xidaki, P. Agrafioti, D. Diomatari, A. Kaminari, E. Tsalavoutas-Psarras, P. Alexiou, V. Psycharis, E.C. Tsilibary, S. Silvestros, M. Sagnou, Synthesis of hydroxyapatite, beta-tricalcium phosphate and biphasic calcium phosphate particles to act as local delivery carriers of curcumin: loading, release and in vitro studies, Materials 11 (4) (2018), https://doi.org/10.3390/ma11040595.

[49] W.E.G. Muller, E. Tolba, H.C. Schroder, R. Munoz-Espi, B. Diehl-Seifert, X. Wang, Amorphous polyphosphate-hydroxyapatite: a morphogenetically active substrate for bone-related SaOS-2 cells in vitro, Acta Biomater. 31 (2016) 358–367, https://doi.org/10.1016/j.actbio.2015.11.060.

[50] V.M. Ramakrishnan, N.L. Boyd, The adipose stromal vascular fraction as a complex cellular source for tissue engineering applications, Tissue Eng. Part B Rev. 24 (4) (2018) 289–299, https://doi.org/10.1089/ten.TEB.2017.0061.

[51] T. Kamenaga, Y. Kuroda, K. Nagai, M. Tsubosaka, Y. Takashima, K. Kikuchi, M. Fujita, K. Ikuta, K. Anjiki, T. Maeda, N. Nakano, K. Takayama, S. Hashimoto, S. Hayashi, T. Matsushita, T. Niikura, R. Kuroda, T. Matsumoto, Cryopreserved human adipose-derived stromal vascular fraction maintains fracture healing potential via angiogenesis and osteogenesis in an immunodeficient rat model, Stem Cell Res. Ther. 12 (1) (2021) 110, https://doi.org/10.1186/s13287-021-02182-3.

[52] A. Todorov, M. Kreutz, A. Haumer, C. Scotti, A. Barbero, P.E. Bourgine, A. Scherberich, C. Jaquiery, I. Martin, Fat-derived stromal vascular fraction cells enhance the bone-forming capacity of devitalized engineered hypertrophic cartilage matrix, Stem Cells Transl. Med. 5 (12) (2016) 1684–1694, https://doi.org/10.5966/sctm.2016-0006.

[53] M. Yu, W. Liu, J. Li, J. Lu, H. Lu, W. Jia, F. Liu, Exosomes derived from atorvastatin-pretreated MSC accelerate diabetic wound repair by enhancing angiogenesis via AKT/eNOS pathway, Stem Cell Res. Ther. 11 (1) (2020) 350, https://doi.org/10.1186/s13287-020-01824-2.

[54] J. Tang, Q. Xie, G. Pan, J. Wang, M. Wang, Mesenchymal stem cells participate in angiogenesis and improve heart function in rat model of myocardial ischemia with reperfusion, Eur. J. Cardio. Thorac. Surg. 30 (2) (2006) 353–361, https://doi.org/10.1016/j.ejcts.2006.02.070.

[55] T.D.X. Tran, V.Q. Pham, N.N. Tran, H.C.N. Dang, N.T.A. Tran, N.B. Vu, P. Van Pham, Stromal vascular fraction and mesenchymal stem cells from human adipose tissue: a comparison of immune modulation and angiogenic potential, Adv. Exp. Med. Biol. (2022), https://doi.org/10.1007/5584_2022_708.

[56] H. Bi, H. Li, C. Zhang, Y. Mao, F. Nie, Y. Xing, W. Sha, X. Wang, D.M. Irwin, H. Tan, Stromal vascular fraction promotes migration of fibroblasts and angiogenesis through regulation of extracellular matrix in the skin wound healing process, Stem Cell Res. Ther. 10 (1) (2019) 302, https://doi.org/10.1186/s13287-019-1415-6.

[57] J.S. Zakhari, J. Zabonick, B. Gettler, S.K. Williams, Vasculogenic and angiogenic potential of adipose stromal vascular fraction cell populations in vitro, In Vitro Cell. Dev. Biol. Anim. 54 (1) (2018) 32–40, https://doi.org/10.1007/s11626-017-0213-7.

[58] Y.J. Koh, B.I. Koh, H. Kim, H.J. Joo, H.K. Jin, J. Jeon, C. Choi, D.H. Lee, J.H. Chung, C.H. Cho, W.S. Park, J.K. Ryu, J.K. Suh, G.Y. Koh, Stromal vascular fraction from adipose tissue forms profound vascular network through the dynamic reassembly of blood endothelial cells, Arterioscler. Thromb. Vasc. Biol. 31 (5) (2011) 1141–1150, https://doi.org/10.1161/ATVBAHA.110.218206.

[59] R.A. Harper, F.M. Pfeiffer, T.J. Choma, The minipig as a potential model for pedicle screw fixation: morphometry and mechanics, J. Orthop. Surg. Res. 14 (1) (2019) 246, https://doi.org/10.1186/s13018-019-1292-9.

[60] C. Weber-Levine, A.M. Hersh, K. Jiang, D. Routkevitch, Y. Tsehay, A. Perdomo-Pantoja, B.F. Judy, M. Kerensky, A. Liu, M. Adams, J. Izzi, J.C. Doloff, N. Manbachi, N. Theodore, Porcine model of spinal cord injury: a systematic review, Neurotrauma Rep 3 (1) (2022) 352–368, https://doi.org/10.1089/neur.2022.0038.

[61] J.K. Burkus, H.S. Sandhu, M.F. Gornet, M.C. Longley, Use of rhBMP-2 in combination with structural cortical allografts: clinical and radiographic outcomes in anterior lumbar spinal surgery, J. Bone Joint Surg. Am. 87 (6) (2005) 1205–1212, https://doi.org/10.2106/JBJS.D.02532.

[62] L. Perez Suarez de Durandeau, M.C. Salinas Carmona, J.G. Silva Siwady, J.R. Hinojosa Ayala, [Chronic mucocutaneous candidiasis. Cutaneous expression of immunologic anomalies. Report of a case], Med. Cutan Ibero Lat. Am. 14 (5) (1986) 357–363.

[63] B. Skovrlj, S.M. Koehler, P.A. Anderson, S.A. Qureshi, A.C. Hecht, J.C. Iatridis, S.K. Cho, Association between BMP-2 and carcinogenicity, Spine (Phila Pa 40 (23) (1976) 1862–1871, https://doi.org/10.1097/BRS.0000000000001126.

[64] A. Hoppe, N.S. Guldal, A.R. Boccaccini, A review of the biological response to ionic dissolution products from bioactive glasses and glass-ceramics, Biomaterials 32 (11) (2011) 2757–2774, https://doi.org/10.1016/j.biomaterials.2011.01.004.

[65] R.P. Phipps, S.H. Stein, R.L. Roper, A new view of prostaglandin E regulation of the immune response, Immunol. Today 12 (10) (1991) 349–352, https://doi.org/10.1016/0167-5699(91)90064-Z.

[66] Y.R. Shih, Y. Hwang, A. Phadke, H. Kang, N.S. Hwang, E.J. Caro, S. Nguyen, M. Siu, E.A. Theodorakis, N.C. Gianneschi, K.S. Vecchio, S. Chien, O.K. Lee, S. Varghese, Calcium phosphate-bearing matrices induce osteogenic differentiation of stem cells through adenosine signaling, Proc. Natl. Acad. Sci. U.S.A. 111 (3) (2014) 990–995, https://doi.org/10.1073/pnas.1321717111.

[67] T. Arahira, M. Todo, Effects of proliferation and differentiation of mesenchymal stem cells on compressive mechanical behavior of collagen/beta-TCP composite scaffold, J. Mech. Behav. Biomed. Mater. 39 (2014) 218–230, https://doi.org/10.1016/j.jmbbm.2014.07.013.

[68] H. Tebyanian, M.H. Norahan, H. Eyni, M. Movahedin, S.J. Mortazavi, A. Karami, M.R. Nourani, N. Baheiraei, Effects of collagen/beta-tricalcium phosphate bone graft to regenerate bone in critically sized rabbit calvarial defects, J. Appl. Biomater. Funct. Mater. 17 (1) (2019) 2280800018820490, https://doi.org/10.1177/2280800018820490.

[69] R. Dimatteo, N.J. Darling, T. Segura, In situ forming injectable hydrogels for drug delivery and wound repair, Adv. Drug Deliv. Rev. 127 (2018) 167–184, https://doi.org/10.1016/j.addr.2018.03.007.

[70] F.M. Chen, M. Zhang, Z.F. Wu, Toward delivery of multiple growth factors in tissue engineering, Biomaterials 31 (24) (2010) 6279–6308, https://doi.org/10.1016/j.biomaterials.2010.04.053.

[71] J. Picchi, L. Trombi, L. Spugnesi, S. Barachini, G. Maroni, G.B. Brodano, S. Boriani, M. Valtieri, M. Petrini, M.C. Magli, HOX and TALE signatures specify human stromal stem cell populations from different sources, J. Cell. Physiol. 228 (4) (2013) 879–889, https://doi.org/10.1002/jcp.24239.

[72] X. Chen, W. Xie, M. Zhang, Y. Shi, S. Xu, H. Cheng, L. Wu, J.L. Pathak, Z. Zheng, The emerging role of non-coding RNAs in osteogenic differentiation of human bone marrow mesenchymal stem cells, Front. Cell Dev. Biol. 10 (2022) 903278, https://doi.org/10.3389/fcell.2022.903278.

[73] D. Logeart-Avramoglou, F. Anagnostou, R. Bizios, H. Petite, Engineering bone: challenges and obstacles, J. Cell Mol. Med. 9 (1) (2005) 72–84, https://doi.org/10.1111/j.1582-4934.2005.tb00338.x.

[74] Y. Gan, K. Dai, P. Zhang, T. Tang, Z. Zhu, J. Lu, The clinical use of enriched bone marrow stem cells combined with porous beta-tricalcium phosphate in posterior spinal fusion, Biomaterials 29 (29) (2008) 3973–3982, https://doi.org/10.1016/j.biomaterials.2008.06.026.

[75] F. Salamanna, M. Sartori, G.B. Brodano, C. Griffoni, L. Martini, S. Boriani, M. Fini, Mesenchymal stem cells for the treatment of spinal arthrodesis: from preclinical research to clinical scenario, Stem Cell. Int. 2017 (2017) 3537094, https://doi.org/10.1155/2017/3537094.

[76] Y. Sun, S. Chen, X. Zhang, M. Pei, Significance of cellular cross-talk in stromal vascular fraction of adipose tissue in neovascularization, Arterioscler. Thromb. Vasc. Biol. 39 (6) (2019) 1034–1044, https://doi.org/10.1161/ATVBAHA.119.312425.

[77] M. Ghiasloo, R.C. Lobato, J.M. Diaz, K. Singh, A. Verpaele, P. Tonnard, Expanding clinical indications of mechanically isolated stromal vascular fraction: a systematic review, Aesthet Surg. J. 40 (9) (2020) NP546–NP560, https://doi.org/10.1093/asj/sjaa111.

[78] F. Saxer, A. Scherberich, A. Todorov, P. Studer, S. Miot, S. Schreiner, S. Guven, L. A. Tchang, M. Haug, M. Heberer, D.J. Schaefer, D. Rikli, I. Martin, M. Jakob, Implantation of stromal vascular fraction progenitors at bone fracture sites: from a rat model to a first-in-man study, Stem Cell. 34 (12) (1981) 2956–2966, https://doi.org/10.1002/stem.2478.

[79] A. Perdomo-Pantoja, C. Holmes, E. Cottrill, A.N. Rindone, W. Ishida, M. Taylor, C. Tomberlin, S.L. Lo, W.L. Grayson, T.F. Witham, Comparison of freshly isolated adipose tissue-derived stromal vascular fraction and bone marrow cells in a

[80] posterolateral lumbar spinal fusion model, Spine (Phila Pa 46 (10) (1976) 631–637, https://doi.org/10.1097/BRS.0000000000003709.

[80] M.J. Dewey, B.A.C. Harley, Biomaterial design strategies to address obstacles in craniomaxillofacial bone repair, RSC Adv. 11 (29) (2021) 17809–17827, https://doi.org/10.1039/d1ra02557k.

[81] M. Potente, H. Gerhardt, P. Carmeliet, Basic and therapeutic aspects of angiogenesis, Cell 146 (6) (2011) 873–887, https://doi.org/10.1016/j.cell.2011.08.039.

[82] Y. Yao, X.H. Xu, L. Jin, Macrophage polarization in physiological and pathological pregnancy, Front. Immunol. 10 (2019) 792, https://doi.org/10.3389/fimmu.2019.00792.